分类号_____密级_____

UDC[注1]_____

中 国 科 学 院

学 位 论 文

题名: 半导体低维结构中子带间电子散射对输运的影响

作者姓名: 董 兵

指导教师: 雷啸霖 研究员

中国科学院上海冶金研究所、上海市长宁路865号

申请学位级别: 博士

专业名称: 半导体物理与半导体器件物理

论文提交日期: 一九九七年一月 论文答辩日期: 一九九七年八月十八日

答辩委员会主席: 吴翔(教授)

评阅人: 吴翔, 刘普林, 李爱珍, 施天生, 汪仲诚

学位授予单位和日期: 中国科学院上海冶金研究所 一九九七年八月十九日

一九九七年一月

注1: 注明《国际十进制分类法UDC》的类号

致谢

首先，衷心地感谢导师雷啸霖研究员三年来的悉心指导与亲切关怀。雷先生简洁而又深刻的物理思想、一丝不苟的治学态度常常给学生以启迪和鞭策，使学生能很愉快地进行工作。

感谢固体物理研究室沈芝霞老师及全室老师、同学在生活和工作上的关心与帮助。

感谢王雪峰、翁小明、束伟民、邹志强、曹俊诚、陈意桥等同学在论文完成过程中的有益讨论和帮助。

感谢研究生部的老师们给予的热情关怀。

最后，特别要感谢我的父母，正是他们二十几年来不断的无私关怀与鼓励促使我坚持不懈地完成自己的学业。

论文摘要

随着半导体生长技术的发展，人们能够制造出在一个及两个维度方向受限的尺寸仅为纳米量级的半导体低维系统，从而实现对半导体能带结构的任意剪裁。由于这些低维系统具有许多新奇的性质，能实现人们对电子器件在功能、速度、集成度等方面的高要求，日益受到人们广泛的重视。

低维半导体结构中电子输运性质的研究是各种器件设计的基础，它已经成为半导体研究领域的一个重要课题。在早期人们主要对量子极限条件下(只考虑最低子带被占据)的低维系统进行了研究。实际上，当电子浓度较高或温度较高时，最低子带以上的子带必然会被电子所占据，从而影响低维系统的输运性质，甚至会导致一些在体材料中观测不到的新现象。近年来随着技术的进一步发展，人们已经在一些输运实验中观测到了上述子带效应。此外，在如此微小的系统上加偏压将产生非常强的电场，电子在强电场加速下通常会很快被加热，电子的输运性质也从线性向非线性过渡，因此研究低维系统的输运性质必须同时考虑多子带及非线性效应。

目前大量研究低维系统输运性质的文章均认为，由于不同子带中的电子具有相同的荷质比，它们可以被作为同一类载流子来处理，从而简化理论描述。上述假定实际上依赖于不同子带电子间的强烈耦合。系统加上电场后，电子从电场获得能量而被加热，如果子带间电子库仑作用足够强，使得不同子带电子之间能够充分交换能量而趋于平衡，那么上述假定是成立的。Goodnick *et.al.* 应用 Monte Carlo 方法模拟了多子带 GaAs-AlGaAs 量子阱中电子-电子相互作用对非平衡输运性质的影响。对一单带系统，他们的模拟显示：与体系统相同，电子-电子相互作用重新分配了电子从电场中获得的能量而使电子趋于平衡状态的 Maxwellian-type 分布。对两子带系统，他们模拟了用激光激发后不同子带电子能量随时间的变化(弛豫)，发现它们在子带间电子库仑相互作用的影响下很快趋于相同。不过此一模拟是在无外加电场条件下的自然弛豫过程，并不能由此推出有外电场时的子带间快速热化的结论。同时，Goodnick 还发现载流子浓度的高低极大地影响电子-电子散射率的大小。如果电子浓度不是很高，在外电场作用下子带间电子-电子散射有可能不足以使处于不同子带的电子之间充分热化，从而不同子带可能维持着不同的能量，拥有不同的电子温度和漂移速度，不同子带的电子不能被简单地当作同一种载流子来处理，因此上述假定有待理论的检验。Monte Carlo 是一个功能强大的纯数值模拟方法，它需要借助

容量极大、速度极快的大型计算机来处理问题，并且难以对整个处理过程有一个清晰而直观的物理解释。所以有必要发展一套效率更高、物理上更直观的方法来研究上述问题。本论文的主要目的就是把适于多种载流子的Lei-Ting平衡方程推广到低维系统，研究子带间电子-电子库仑散射对系统输运性质的影响。

众所周知，对一简单抛物能带系统，考虑一个能带内的电子输运问题，如果忽略U过程，那么由于平移不变性电子-电子散射的作用仅仅是在电子之间重新分配动量(热化)而总动量保持不变，因此电子-电子散射不会对输运产生直接的影响。当然，如果平移不变性被破坏，系统的输运参数必然有电子-电子散射的直接贡献部分。比如，最近Messica *et al.* 在GaAs-AlGaAs表面超晶格(surface superlattice)中观察到了电子-电子散射对电阻的直接贡献，这正是由于超晶格中微带(miniband)的形成改变了系统的简单抛物能带结构，从而破坏了平移不变性引起的。另外一种方法是靠近原系统引入另一电子系统，两系统通过库仑作用而相互关联，动量由于库仑作用可以在系统间相互传递，因此我们可以观察到系统间库仑作用在单个系统的输运性质上留下的印记。例如，人们很早就认识到的过渡族金属起源于s带与d带电子库仑耦合的T^2(三维)及$T^2 \ln T$(二维)低温电阻温度行为；GaAs-AlGaAs量子阱中电子-空穴牵引效应引起的少子负迁移率；以及最近大量研究的耦合阱间的库仑牵引现象，它指的是两个非常靠近但没有粒子交换的电子子系统中，其中一个子系统(主动子系统)的电子运动可以通过库仑作用使另一个子系统(被动子系统)产生电流或电场。现在所关心的单量子阱多子带系统正是这样的情形，其子带间电子库仑相互作用对系统的输运性质应该有直接的影响。

传统的玻耳兹曼方程两带模型可以很好地描述上述过渡族金属低温电阻温度行为及耦合阱间的库仑牵引现象，但是对单量子阱多子带系统，由于不同子带电子具有相同的荷质比，它得出子带间电子库仑相互作用对线性电阻贡献为零的结论。而且，玻耳兹曼方程理论局限于线性输运，对非线性输运难以适用。近十年来发展起来的雷-丁平衡方程理论把电场作用下的多电子运动化为单电子质心的力学运动和相对电子的统计运动，导致了非线性输运的简洁描述，成为输运研究中非常有效的方法。由原始的雷-丁平衡方程发展而来的适用于多谷半导体系统多种载流子输运的平衡方程已经被用来处理量子阱中电子-空穴的库仑牵引及耦合阱间的库仑牵引问题，对后者的处理得到与玻耳兹曼方程两带模型完全相同的结论。本文进一步把它发展到适合低维系统多子带多种载流子输运情形。与玻耳兹曼方程两带模型不同，多种载流子平衡方程中的子带间库仑作用并不会由

于相同的荷质比而消失。多种载流子平衡方程是合适的研究子带间热化的理论模型。

利用此模型研究低维系统子带间库仑相互作用对线性及非线性输运性质的影响。考察了载流子浓度对子带间热化的决定性作用，指出当电子浓度提高时，子带间电子库仑作用增强，使得不同子带电子之间可以充分交换能量而达到平衡，此时不同子带电子可以被作为同一种载流子处理，并使计算得以简化。研究了不同子带间电子库仑作用强度条件下的线性迁移率。弱电子-电子作用极限下的迁移率正是玻耳兹曼方程两带模型的结果 μ_B，这与上文的讨论是一致的；对强电子-电子极限，物理直观告诉我们此时不同子带电子总是充分热化的，迁移率应当与一种载流子平衡方程的迁移率等价 μ_L；以及介于两者之间的真实迁移率。同时给出一个观察迁移率从 μ_B 向 μ_L 变化的实验方案。

最后，关于不同子带化学势及占据数的研究，指出了目前这一模型的缺陷。由于在考虑子带间库仑作用时忽略了较次要的与子带间粒子交换有关的量，导致子带化学势无法象电子温度与漂移速度那样随电子浓度的增高而趋于一致。因此如何完善现有模型，使之能考虑与子带间粒子交换有关的库仑作用是我们下一步工作的目标。

另外，我们还利用平衡方程方法研究了GaAs-AlGaAs异质结在多子带占据条件下的低频热噪声温度及超晶格中空穴的纵向Bloch输运，得到一些新奇的输运性质。

Intersubband Coulomb Scattering Effect on Transport in semiconductor Low-dimensional Systems

Abstract

The effect of the inersubband electron-electron Coulomb interaction on the linear and nonlinear transport properties in GaAs-based low-dimensional systems in the case of multisubband occupied is investigated systematically by means of the Lei-Ting balance-equations approach using a model with multiple types of carriers (MTCM). A clear signature of the intersubband electron-electron Coulomb interaction in the linear mobility is demonstrated. At the high electric field regime, enough high electon density can enhace drastically the intersubband Coulomb interaction and hence make electrons among different subbands reach rapidly equilibrium state, in which electrons within different subbands can be treated as one type of carriers. The thermal noise temperature is evaluated for quasi-two-dimensional heterojunctions considering two subbands occupied. By employing the developed balance-equations theory for Bloch miniband transport, we invesitgate in detail the hole vertical transport in superlattices including the effect of heavy-hole–light-hole mixing, exhibiting novel density-dependence of linear mobility and break-down of the negative differential velocity in velocity-field curves.

Contents

1 **Introduction** 3

2 **Effects of Inter-subband Coulomb Interaction on Electron Transport in Low-dimensional Systems** 7
- 2.1 Background . . . 7
- 2.2 Balance Equation Theory for Electron Transport in Semiconductor Systems with Two Types of Carriers . . . 9
- 2.3 Electron Transport in Quantum Wells . . . 13
- 2.4 Electron Transport in Quantum Wires . . . 16
- 2.5 Discussion . . . 19
  - 2.5.1 Dependence on Carrier Density . . . 19
  - 2.5.2 Dependence on the Confinement . . . 22
  - 2.5.3 Chemical Potential and Subband Occupancy under External Electric Fields . . . 23
  - 2.5.4 Intersubband Coulomb Scattering in Linear Mobility in Quantum Wells . . . 26
- 2.6 Conclusion . . . 28

3 **Electron Noise Temperature in Heterjunction** 29
- 3.1 Background . . . 29
- 3.2 Electron Transport in Heterojunctions for the Two-Sub-band Occupied Case . . . 30
- 3.3 Balance Equation Theory for Thermal Noise Temperature . . . 32
- 3.4 Electron Noise Temperature in Heterojunction for the Two-subband Occupied Case . . . 34

4 **Hole Perpendicular Transport of Superlattice Systems** 38
- 4.1 Background . . . 38
- 4.2 Balance Equation Theory for an Arbitrary Energy Band . . . 39
- 4.3 Hole Bloch Transport in Superlattices . . . 41
- 4.4 Discussion . . . 43

5 **Summary** 46

Chapter 1

Introduction

Recent progress in crystallographic growth techniques makes the two-dimensional electron gas (2DES) in high mobility GaAs-AlGaAs heterostructure and quantum well become an especially suitable system for studying electron-electron interaction effects, because of the reduced effect of impurity scattering arising from the modulation-doping technique. Electron-electron interactions play an important role in systems of this reduced dimensionality. They are, for example, responsible for the existence of the fractional quantum Hall effect and Wigner solid states of the 2DES. Artifacts of electron-electron interactions can also be observed in other way in the 2DES, such as the negative magnetoresistance often seen in magnetic fields around 1 T, the oscillatory behavior of the g factor, valley splitting, Landau-level width and the negative density of states (negative compressibility of electrons). Besides, an area of active research to this day, both experimentally[1, 2] and theoretically[3, 4], is the effect of electron-electron interactions on transport and/or the Coulomb inelastic-scattering time (quasiparticle lifetime)[5–8] in bulklike systems of various dimensionalities.

It is well-known[9, 10] that in the case of semiconductors with a single isotropic parabolic band, electron-electron scattering should not directly affect the transport properties of bulklike systems (purely quantum effects such as weak-localization corrections excepted) since in the absence of Umklapp processes an electron-electron scattering event only redistributes the momentum of the electron gas and conserves its total value in the system due to the translation invariance of the phase-space. Of course, on the other hand, this fact suggests us that the effect of electron-electron interaction can be directly observed in transport experiments if the translational invariance of phase-space is broken down in the system. There are two ways to do this. One is to change the single band structure of the system to a profound and extremely nonparabolic band. It is should be noted that this way is easy to understand in physical concept but difficult to manipulate in technique. Recently, Messica *et al.*[11] have experimentally confirmed the idea. They have presented transport measurements on surface superlattices fabricated on a GaAs-AlGaAs 2DES and observed a direct contribution of electron-electron scattering on the resistance due to the loss of translational invariance and the formation of minibands.

The other way is to add other system so close to the original system that the charges in two respective systems experience the Coulomb forces, which leads to momentum transfer between the two systems. Even though the total value of momentum still keeps constant because of the nature of electron-electron scattering, momentum of electrons in a system can be transfer to another by inter-system Coulomb interaction and the transport properties of the individual system can be influenced. Thus this causes changing of transport properties. It has been appreciated for a long time that the resistivity behaving as T^2 for a three-dimensional electron gas[12] and as $T^2 \ln T$ at two dimensions[5, 13] indeed results from Coulomb coupling of conduction s electron to a narrow d band in transition metals. Negative minority-carrier mobility in GaAs-AlGaAs quantum wells[14, 15] experimentally observed by Höpfel and collaborators is attributed to the associated carrier-drag effect between the electron subband and hole subband in an electric field. In a flurry of recent experiments and theoretical works,

drag between two spatially separated and coupled 2DES systems due to Coulomb interactions between carriers have been intensively investigated[16–19]. If a current is driven through one of the systems, then an induced current is dragged in the other system. Moreover, even for a single low-dimensional systems, the formation of subbands due to confinment opens new scattering channels, inter-subband scatterings, including inter-subband carrier-carrier Coulomb interactions, to affect transport properties. The above mentioned Höpfel's experiment about carrier-drag effect is an example. However, different from the large disparity of effective masses between electron and hole, electrons populated in different subbands have a common effective mass, hence are assumed to possess a common energy even under a strong electric field in the literature and inter-subband Coulomb interactions do not directly affect transport. In fact, the presumption is based upon enough large intersubband electron-electron Coulomb interaction to induce rapid thermalization of the carriers and its validity in linear and nonlinear cases is still a question to be deliberately explored. Nevertheless, so far, the inter-subband thermalization due to Coulomb interaction has been less investigated. Goodnick *et al.*[20] simulated the intra- and intersubband electron-electron scatterings on nonequilibrium transport in quantum-well systems unsing ensembel Monte Carlo approach and argued that intersubband energy exchange due to Coulomb scattering largely depends on the carreir density and is strong enough to equalize the subband energies for the simulated systems. This pure numerical method is not only large time consuming, but also lack of intuitively clear approximation scheme. And these shortcomings pronounced more in dealing with electron-electron scatterings, which invoke one to develop a computationally more effective and physically more intuitive approach.

The conventional treatment of transport properties is based on Boltzmann equation in which the electron-electron scattering can be intuitively treaed as Boltzmann's collision term. The Boltzmann equation for the single particle distribution function $f(\mathbf{k},\mathbf{r},t)$ of the electrons can be written in the usual form

$$\left[\frac{\partial}{\partial t}+\mathbf{v}(\mathbf{k})\cdot\nabla_{\mathbf{r}}-e\mathbf{E}\cdot\nabla_{\mathbf{k}}\right]f(\mathbf{k},\mathbf{r},t)=\left(\frac{\partial f(\mathbf{k},\mathbf{r},t)}{\partial t}\right)_{c}$$

where $\mathbf{v}(\mathbf{k})=\nabla_{\mathbf{k}}\varepsilon_{\mathbf{k}}$ is electron group velocity and $\mathbf{E}$ is applied electric field. The introduction of the concept of an electron state of wavevector $\mathbf{k}$ indicates that the one-electron approximation is used, closely connected with this approximation is the energy $\varepsilon_{\mathbf{k}}$ of the state $\mathbf{k}$ as a function of $\mathbf{k}$. The collisional term $(\partial f/\partial t)_c$ is given by

$$\left(\frac{\partial f(\mathbf{k},\mathbf{r},t)}{\partial t}\right)_{c}=\sum_{\mathbf{k}'}\left\{\Gamma(\mathbf{k}',\mathbf{k})-\Gamma(\mathbf{k},\mathbf{k}')\right\},$$

where

$$\Gamma(\mathbf{k},\mathbf{k}')=W(\mathbf{k},\mathbf{k}')f(\mathbf{k})\left[1-f(\mathbf{k}')\right]$$

is the transition rate from from the state $\mathbf{k}$ to the state $\mathbf{k}'$ and $W(\mathbf{k},\mathbf{k}')$ is transition probability as a result of scatterings by impurities, phonons. However, in contradistinction to the elastic scattering of electrons by impurities and to the emission and absorption of phonons, electron-electron interactions give rise to *two-particle scattering processes*. The transition rate and the collision term can be generalized to the case of two-particle collisions as the respective form,[10]

$$\Gamma(\mathbf{kp},\mathbf{k}'\mathbf{p}')=W(\mathbf{k},\mathbf{k}')f(\mathbf{k})\left[1-f(\mathbf{k}')\right]f(\mathbf{p})\left[1-f(\mathbf{p}')\right],$$

and

$$\left(\frac{\partial f(\mathbf{k},\mathbf{r},t)}{\partial t}\right)_{e\text{-}e}=\sum_{\mathbf{k}'\mathbf{p}\mathbf{p}'}\left\{\Gamma(\mathbf{k}'\mathbf{p}',\mathbf{kp})-\Gamma(\mathbf{kp},\mathbf{k}'\mathbf{p}')\right\}.$$

Then by solving the linearized Boltzmann equation, the Coulomb interaction induced resistivity tensor

can be derived as

$$\rho_{\alpha\beta} \propto \sum_{\mathbf{kpq}} |V_c(q)|^2 f(\varepsilon_{\mathbf{k}}) f(\varepsilon_{\mathbf{p}}) \left(1 - f(\varepsilon_{\mathbf{k+q}})\right) \left(1 - f(\varepsilon_{\mathbf{p-q}})\right) \delta\left(\varepsilon_{\mathbf{k}} + \varepsilon_{\mathbf{p}} - \varepsilon_{\mathbf{k+q}} - \varepsilon_{\mathbf{p-q}}\right) \times \left(\mathbf{v}_{\mathbf{k}} + \mathbf{v}_{\mathbf{p}} - \mathbf{v}_{\mathbf{k+q}} - \mathbf{v}_{\mathbf{p-q}}\right)_{\alpha} \left(\mathbf{v}_{\mathbf{k}} + \mathbf{v}_{\mathbf{p}} - \mathbf{v}_{\mathbf{k+q}} - \mathbf{v}_{\mathbf{p-q}}\right)_{\beta} ,$$

where $f(\varepsilon_{\mathbf{k}})$ is the Fermi-Dirac distribution function for energy $\varepsilon_{\mathbf{k}}$. It follows immediately from the one-band resistivity formula that for a single parabolic band $\mathbf{v}_{\mathbf{k}} \propto \mathbf{k}$, the Coulomb interaction gives zero resistance in absence of Umklapp processes. But this is not the case for the lateral surface superlattice, in which the energy and velocity are a nontrivial function of $\mathbf{k}$. The results are in agreement with above qualitative discussions. In the standard two-band model,[10] Boltzmann equation yields the inter-band Coulomb interaction induced resistivity tensor of system 1 as

$$\rho^{(1)}_{\alpha\beta} \propto \sum_{\mathbf{kpq}} |V_c(q)|^2 f(\varepsilon_{1\mathbf{k}}) f(\varepsilon_{2\mathbf{p}}) \left(1 - f(\varepsilon_{1\mathbf{k+q}})\right) \left(1 - f(\varepsilon_{2\mathbf{p-q}})\right) \delta\left(\varepsilon_{1\mathbf{k}} + \varepsilon_{2\mathbf{p}} - \varepsilon_{1\mathbf{k+q}} - \varepsilon_{2\mathbf{p-q}}\right) \times \left(\psi_{1\mathbf{k}} + \psi_{2\mathbf{p}} - \psi_{1\mathbf{k+q}} - \psi_{2\mathbf{p-q}}\right)_{\alpha} \left(\psi_{1\mathbf{k}} + \psi_{2\mathbf{p}} - \psi_{1\mathbf{k+q}} - \psi_{2\mathbf{p-q}}\right)_{\beta} ,$$

and similarly for $\rho^{(2)}_{\alpha\beta}$, where the deviation function ψ is defined by $f - f^0 = f^0(1 - f^0)\psi$. This model has been used in the literature to calculate the transresistivity in coupled quantum wells.[19] The theoretical results is in significant agreement with experiments, which showes that the two-band formula is a applicable model for the Coulomb-drag phenomena. However, it does not work for the intersubband electron-electron collision in a single quantum well. Meanwhile, Boltzmann equation is believed to be formidable to deal with transport beyond linear regime.

A decade of years ago, Lei and Ting[21] developed a new balance-equations approach to nonlinear electric transport for an electron-phonon-impurity system, which is believed to be valid for systems with strong electron-electron interactions in contrast to the Boltzmann equation for the weak electron-electron interactions regime.[22, 23] Basing on the separation of the center-of-mass motion from the relative motion of electrons in Hamiltonian and in density matrix, the system can be considered to have two parts: the center-of-mass, which is a single particle having an enormous mass, and the relative electron system, which contains a large number of electrons forming a statistical ensemble. The fact that external electric field acts only on the center-of-mass and the relative electron system coulpes with the center-of-mass and the lattice only through the electron-impurity and electron-phonon interactions make it possible to treat the center-of-mass as a classical particle with a constant velocity $\mathbf{v}_d$ and to introduce an electron temperature T_e for the decoupled nonequilibrium relative electron system as a measurement of its internal energy. To the first order of electron-impurity and electron-phonon interactions a set of force and energy balance equations are derived. Although the original balance-equations approach is derived for one type of carriers moving in a single parabolic band, it has been extended to the systems with nonparabolic energy band[24] and/or multivalley[25, 26]. Treating the intervalley Coulomb scattering as a perturbation along with the electron-impurity and electron-phonon interactions, the force $\mathbf{f}_{12}$ and energy transfer rate w_{12} due to intervalley Coulomb interaction can be easily determined as the following forms[25]

$$\mathbf{f}_{12} = \sum_{\mathbf{q}} |V_c(\mathbf{q})|^2 \, \mathbf{q} \int_{-\infty}^{\infty} \frac{d\omega}{\pi} \left[n\left[\frac{\omega}{T_{1e}}\right] - n\left[\frac{\omega - \omega_{12}}{T_{2e}}\right] \right] \Pi_2^{(1)}(\mathbf{q},\omega) \Pi_2^{(2)}(\mathbf{q},\omega - \omega_{12}). \qquad (1.1)$$

and

$$w_{12} = \sum_{\mathbf{q}} |V_e(\mathbf{q})|^2 \int_{-\infty}^{\infty} \frac{d\omega}{\pi} \omega \left[n\left[\frac{\omega}{T_{1e}}\right] - n\left[\frac{\omega-\omega_{12}}{T_{2e}}\right] \right] \Pi_2^{(1)}(\mathbf{q},\omega)\Pi_2^{(2)}(\mathbf{q},\omega-\omega_{12}),$$

with $\omega_{12} \equiv \mathbf{q}\cdot(\mathbf{v}_1 - \mathbf{v}_2)$, respectively.

Applying the balance-equations approach for several types of carriers systems, Lei *et al.*[27] have investigated the steady-state nonlinear dc and linear high frequency transport properties of type-II superlattices, focusing on the electron-hole scattering mechanism. This approach has been also employed to analyze carrier transport for a two-component plasma consisting of minority electrons and majority-holes ($N_e \ll N_h$) in a GaAs-AlGaAs quantum well[28]. Numerical results for Ohmic mobilities as functions of lattice temperature and for nonlinear mobilities as functions of applied electric field strength are in good agreement with the experimental data of Höpfel *et al.*. The recent hot-focused Coulomb drag effec is another example which this balance-equations approach can deal with[29]. The tranresistivity can be readily recognized from the low velocity limit of the Eq.(1.1)

$$\rho_{12} = \frac{1}{N_1 N_2 e^2 T} \sum_{\mathbf{q}} q^2 |V_{12}(q)|^2 \int_0^{\infty} \frac{d\omega}{\pi} \left[e^{\frac{\omega}{2T}} n\left[\frac{\omega}{T}\right] \right]^2 \Pi_2^{(1)}(\mathbf{q},\omega)\Pi_2^{(2)}(\mathbf{q},\omega-\omega_{12}),$$

which is completely identical to the formula derived from other methods, for example, the two-band model of Boltzmann equation above mentioned. Moreover, the Coulomb drag effect between two quantum wells and two laterally confined quantum wells in the presence of a large magnetic field has been studied by the means of the extended formation of this approach with magnetic fields.[30] The theoretical results that the Landau quantization of electron energy can greatly enhance the drag effect are proved by a recent experiment[31] where a strong magnetic field increases the drag effect by 50-100 times.

The main aim of this thesis is to extend the balance-equations approach for several types of carriers systems to low-dimensional systems with multi-subband occupancy and to investigate the effect of intersubband electron-electron Coulomb interaction on linear and nonlinear transport properties in the case of different electron densities and confinements. We can find that, differen from the two-band model of Boltzmann, the Coulomb force Eq.(1.1) can directly contribute to the linear mobility of a single quantum well, which enable us to incorporate electron-electron scattering in linear mobility. Meanwhile, we can use the approach to study the detail of intersubband thermalization resulted from intersubband electron-electron Coulomb interaction and to find out its decisive factors.

The balance-equations theory has been applied in many areas of transport in semiconductors[2], for example, thermal noise[52, 53], which is an important problem in semiconductor and a crucial factor of the reliability of the device[50, 51]. The famous Nyquist relation of thermal noise is based on the linear response theory and is invalid at high-field region. Because the balance-equations theory bears no relation to the strength of the applied electric field, not only the Nyquist relation is re-obtained at low fields, but a modified expression can be derived at high fields from the theory. In Chap.3, we calculate the longitudinal and transverse low-frequency thermal noise temperatures at different electric fields in quasi-two-dimensional heterojunctions considering two subbands occupied.

Miniband transport in superlattice is another hot focus in recent literature. Years ago, Esaki and Tsu[56] predicted that the existence of minibands results in Bloch oscillation and a negative differential velocity (NDV) at electric-field values that can be easily achieved experimentally. Recently, the balance-equations theory has been successfully developed by Lei to study the miniband transport[59]. In Chap. 4, employing the developed balance-equations theory for Bloch miniband transport, we invesitgate in detail the hole vertical transport in superlattices including the effect of heavy-hole-light-hole mixing. We find that the mobilities and velocity-field curves are drastically modified by the profound energy spectrum, exhibiting a break-down of NDV.

Chapter 2

Effects of Inter-subband Coulomb Interaction on Electron Transport in Low-dimensional Systems

2.1 Background

Recently there has been a resurgence of interest in the propertites of high carrier density two-dimensional electron gas systems, looking at the manner in which the second subband is populated, the relative mobilities and scattering times of electrons in the two subbands, and the nature of the intersubband scattering. Much experimental and theoretical attention has been payed to the transport properties of low-dimensional systems, such as quantum wells and quantum wires, under multisubband occupations of carriers because the design of optimised high mobility and high carrier-density devices needs the detailed information about the scattering rate associated with intersubband transitions.[32]

In as early as 1979, Mori and Ando[33] studied the intersubband scatterings effect on the linear mobility of a Si(100) iversion layer at low temperature. Fletcher *et al.*[34] reported on simultaneous measurements of mobility and presented evidence of a mobility edge in the second subband of a GaAs-based heterojunction. Recently, Hamilton *et al.*[35] have presented experimental investigations of the transition from one- to two-subband occupancy in the two-dimensional electron gas (2DES) of back gated modulation-doped GaAs-AlGaAs heterostructures. Their experiment has clearly demonstrated that when only one subband is occupied, the mobility is limited by remote ionized impurity scattering and increase monotonically with increasing carrier density. However, when the Fermi energy approaches the bottom of the second subband , an additional (intersubband) scattering channel is opened up, which causes the 2DES mobility to drop sharply. Subsequently, as the second subband becomes populated, the mobility resumes its monotonic increase with increasing carrier density. Tsuchiya and Ando[36] have theoretically demonstrated a wave-function modulation induced by insertion of several thin barrier layer inside a quantum well can enhance the electron mobility for appropriate values of the parameters for which intersubband scattering proccesses are suppressed. In high electric field, electrons begin to occupy higher subbands and naturally intersubband scattering becomes a important factor to influence the hot electron transport. Lei has extended the Lei-Ting balance equations theory to study nonlinear electron transport in GaAs-AlGaAs heterojunctions[37], taking into account the occupation of the lowest and next lowest subbands and the intrasubband and intersubband Coulomb interactions through RPA dielectric function[38]. Monte Carlo simulations have been performed for hot electron transport in GaAs-based quasi-two-dimensional systems in the case of multivalley and multisubband by many authors[39]. The intersubband scattering plays also a great role in electron transport in quantum wire systems, as demonstrated by Wang. He has systematically studied sub-

band effects on hot electron transport in GaAs-based quantum wires by means of Lei-Ting balance equations theory.[40]

However, in most of investigations on the problem of intersubband scattering, interests are focused on the intersubband electron-phonon interactions[38–44]. In addition, there is a presumption in the literature that electron populated in different subbands share a common energy even at the nonlinear transport regime, which is based on the rapid thermalization of electrons among different subbands. In principle, if intersubband Coulomb scatterings, which effectively transfer energy between different subbands, are strong enough that carriers are thermalized within a much more shorter time than the average momentum relaxation time under an external electric field, the validity of the presumption can be established for these systems [45]. Most of authors believed it to be true without proving because the carriers in different subbands have the same mass and charge. For example, in most balance-equations investigations on transport, electrons in different subbands are assumed to be one-type-of-carriers, i.e., to share a common electron temperature, chemical potential and average drift velocity, even though an external electric field is added[38, 40]. Goodnick and Lugli[20] have studied the effect of electron-electron scattering on nonequilibrium transport in quatum well systems using ensemble Monte Carlo simulation of the full multisubband systems. Their calculation has shown that the intrasubband electron-electron Coulomb interaction can exchange energy between carriers thus redistributing the energy gained by an electric field and driving the electron steady-state distribution function towards a equilibrium-type distribution. Therefore, it is reasonable that electrons in each subband share a unique energy, respectively. Furthermore, their results for the carrier evolution under laser excitation have demonstrated that the electron-electron scattering rate depends substantially on the electron density. That is to say, the above presumption may be invalid if the electron density is not high enough and needs detailed investigation.

Recently, C. Guillemot et al.[42] studied the electron-longitudinal-optical-phonon coupling and intersubband scattering in modulation-doped quantum wells by means of Lei-Ting balance-equations approach, assuming that electrons in the two subbands share a common electron temperature and average drift velocity but have different chemical potentials. Wu and his coworks[46] analyzed transport in quantum-wire system considering the lowest two subbands 0, 1 and its degenerate subband -1 occupied, using a description which is similar to the two-types-of-carriers model (TTCM) used to solve the transport problem of multi-valley bulk materials,[25] in which of model electrons within different valleys and subbands are assumed to have their own electron temperatures, drift velocities (energies) and chemical potentials respectively. Their calculation displayed a little difference from that of the one-type-of-carriers model (OTCM), such are attributed to the intersubband Coulomb interaction included in their literature. This manifested that the intersubband Coulomb interaction is really strong enough to make the subband energies tend to equilibtate for the quantum wires at the carrier density investigated. If this is generally true, the OTCM would be a much more attractive model for the low-dimensional device simulation [47] than the TTCM because the latter requires a much heavier CPU cost. However, the above favorite result is for a special system with a special carrier densities. The systematic theoretical investigation on the validity of the OTCM for low-dimensional multisubband systems in linear and nonlinear transport regime, is still lacking.

Therefore it is desirable to systematically investigate the effect of intersubband scatterings, especially the intersubband electron-electron Coulomb interaction, on the linear and nonlinear transport properties for systems of different dimensionality and having different carrier densities of quasi-two-dimensional and quasi-one-dimensional electron systems.

We[48] employ the Lei-Ting balance-equations approach of two-types-of-carriers model (TTCM)[25] to treat the GaAs-based model systems having two subbands and composed of two types of carriers. The theoretical framework on the Lei-Ting balance-equation approach will be formulated in Sec.2, and we will apply the approach to quasi-two-dimensional quantum wells, and quasi-one-dimensional quantum wires in the following sections. Finally, the numerical calculation and discussion will be presented.

2.2 Balance Equation Theory for Electron Transport in Semiconductor Systems with Two Types of Carriers

Consider a model low-dimensional system, having N electrons under the influence of a uniform applied electric field $\mathbf{E}$. For simplicity, we assume that only the ground and the first excited subbands are occupied in the low-dimensional system and electrons in the two subbands have a common effective electron mass under the effective mass approximation. Those electrons within a subband share a common temperature, average drift velocity and chemical potential due to strong enough intra-subband electron-electron Coulomb interactions. But for electrons dewelling in different subbands, temperatures, average drift velocities and chemical potentials are different. Therefore we have a system composed of two types of carriers. The numbers of carriers in the ground and the first excited subbands are N_1 and N_2 respectively. So, the total number of these carriers is $N = N_1 + N_2$, which is assumed to be constant. However, the numbers of carrier particles of systems 1 and 2, N_1 and N_2, are variable in the presence of a uniform electric field since the carriers in systems 1 and 2 can exchange with each other. We introduce the coordinate $\mathbf{R}$ for the center of mass of the whole system, and $\mathbf{R}_1$ and $\mathbf{R}_2$ for systems 1 and 2:[25]

$$\mathbf{R} = \frac{1}{N}\left[\sum_i^1 \mathbf{r}_{1i} + \sum_i^2 \mathbf{r}_{2i}\right] = (N_1/N)\,\mathbf{R}_z 1 + (N_2/N)\,\mathbf{R}_2, \tag{2.1}$$

and momenta $\mathbf{P}_1$ and $\mathbf{P}_2$ for systems 1 and 2:

$$\mathbf{P}_1 = \sum_i^1 \mathbf{p}_{1i}, \qquad \mathbf{P}_2 = \sum_i^2 \mathbf{p}_{2i}. \tag{2.2}$$

Here $\mathbf{r}_{1i}$, $\mathbf{p}_{1i}$ ($\mathbf{r}_{2i}$, $\mathbf{p}_{2i}$) are coordinates and momenta of the ith particle in system 1 (2), which satisfy the well-known commutation relation $\left[r_{1i}^{\alpha}, p_{1i}^{\beta}\right] = i\delta_{ij}\delta_{\alpha\beta}$, $\left[r_{2i}^{\alpha}, p_{2i}^{\beta}\right] = i\delta_{ij}\delta_{\alpha\beta}$. We also introduce the velocities $\mathbf{v}_1$ and $\mathbf{v}_2$ for the centers of mass of the systems 1 and 2:

$$\mathbf{P}_1 = N_1 m\mathbf{v}_1, \qquad \mathbf{P}_2 = N_2 m\mathbf{v}_2. \tag{2.3}$$

The relative coordinates and momenta for the carrier systems 1 and 2 are defined as

$$\mathbf{r}'_{1i} = \mathbf{r}_{1i} - \mathbf{R}_1, \qquad \mathbf{r}'_{2i} = \mathbf{r}_{2i} - \mathbf{R}_2, \tag{2.4}$$

$$\mathbf{p}'_{1i} = \mathbf{p}_{1i} - m\mathbf{v}_1, \qquad \mathbf{p}'_{2i} = \mathbf{p}_{2i} - m\mathbf{v}_2. \tag{2.5}$$

According to definitions (1) and (2), $[N_1 R_{1\alpha}, P_{1\beta}] = iN_1\delta_{\alpha\beta}$. Therefore it is consistent to consider $\mathbf{R}_1$, $\mathbf{P}_1$ as canonical variables of the center of mass satisfying

$$[R_{1\alpha}, P_{1\beta}] = i\delta_{\alpha\beta}, \tag{2.6}$$

and $\hat{N}_1$, the particle number of system 1, as a variable of the relative electron system 1, which commutes with c.m. variables. It is easily seen that to the order of $O(1/N)$ the relative electron variables $\mathbf{r}'_{1i}$ and $\mathbf{p}'_{1i}$ obey the canonical commutation relation

$$\left[r_{1i}^{\prime\alpha}, p_{1i}^{\prime\beta}\right] = i\delta_{\alpha\beta}\left[\delta_{ij} + O\left[\frac{1}{N_1}\right]\right]. \tag{2.7}$$

Therefore, most of the discussions in Ref. [25] can still apply in the present case. In terms of these new variables the total Hamiltonian of the system in the presence of a uniform electric field $\mathbf{E}$ can be written as follows:

$$\begin{aligned} H &= H_{\rm c.m.E} + H_{\rm c.m.T} + H_{1e} + H_{2e} + H_{ph} + H_I, \\ H_I &= H_{12} + H_{1e-i} + H_{2e-i} + H_{1e-ph} + H_{2e-ph} + H^{12}_{e-ph} + H^{21}_{e-ph}. \end{aligned} \tag{2.8}$$

Here

$$H_{\rm c.m.E} = -Ne\mathbf{E}\cdot\mathbf{R}, \tag{2.9}$$

and

$$H_{\rm c.m.T} = \frac{1}{2}m\hat{N}_1\mathbf{v}_1^2 + \frac{1}{2}m\hat{N}_2\mathbf{v}_2^2 \tag{2.10}$$

are the center-of-mass part of the Hamiltonian. Particle numbers $\hat{N}_1$ and $\hat{N}_2$ can be expressed in the second quantization representation of the relative carrier systems 1 and 2 as

$$\hat{N}_1 = \sum_{\mathbf{k},\sigma}^{1} c^\dagger_{1\mathbf{k}\sigma}c_{1\mathbf{k}\sigma}, \qquad \hat{N}_2 = \sum_{\mathbf{k},\sigma}^{2} c^\dagger_{2\mathbf{k}\sigma}c_{2\mathbf{k}\sigma}, \tag{2.11}$$

where $c^\dagger_{i\mathbf{k}\sigma}$ ($c_{i\mathbf{k}\sigma}$) are creation (annihilation) operators of wave vector $\mathbf{k}$ for the ith ($i = 1, 2$) type of carriers relative to their respective center of mass. H_{1e} and H_{2e} are the relative part of the Hamiltonian for the first and the second carrier systems, including their ("intrasubband") Coulomb interaction:

$$H_{1e} = \sum_{\mathbf{k},\sigma}^{1} \varepsilon_{1\mathbf{k}} c^\dagger_{1\mathbf{k}\sigma}c_{1\mathbf{k}\sigma} + \frac{1}{2}\sum_{\substack{\mathbf{k},\mathbf{k}_1,\mathbf{q}\\ \sigma,\sigma_1}} V_{1c}(\mathbf{q}) c^\dagger_{1\mathbf{k}+\mathbf{q}\sigma} c^\dagger_{1\mathbf{k}_1-\mathbf{q}-\sigma_1} c_{1\mathbf{k}_1\sigma_1} c_{1\mathbf{k}\sigma}, \tag{2.12}$$

$$H_{2e} = \sum_{\mathbf{k},\sigma}^{2} \varepsilon_{2\mathbf{k}} c^\dagger_{2\mathbf{k}\sigma}c_{2\mathbf{k}\sigma} + \frac{1}{2}\sum_{\substack{\mathbf{k},\mathbf{k}_1,\mathbf{q}\\ \sigma,\sigma_1}} V_{2c}(\mathbf{q}) c^\dagger_{2\mathbf{k}+\mathbf{q}\sigma} c^\dagger_{2\mathbf{k}_1-\mathbf{q}-\sigma_1} c_{2\mathbf{k}_1\sigma_1} c_{2\mathbf{k}\sigma}, \tag{2.13}$$

in which $V_{1c}(\mathbf{q})$ and $V_{2c}(\mathbf{q})$ are the intra-the-first-subband and intra-the second-subband Coulomb potentials respectively. In Eq.(2.8) H_{1e-i}, $H_{1e-\rm ph}$, H_{2e-i}, and $H_{2e-\rm ph}$ are electron-impurity and electron-phonon couplings for type-1 and type-2 carriers, respectively:

$$H_{1e-i} = \sum_{\mathbf{q},a} u_1(\mathbf{q}) e^{i\mathbf{q}\cdot(\mathbf{R}_1-\mathbf{R}_a)}\rho_{1\mathbf{q}}, \tag{2.14}$$

$$H_{2e-i} = \sum_{\mathbf{q},a} u_2(\mathbf{q}) e^{i\mathbf{q}\cdot(\mathbf{R}_2-\mathbf{R}_a)}\rho_{2\mathbf{q}}, \tag{2.15}$$

$$H_{1e-\rm ph} = \sum_{\mathbf{q},\lambda} M_1(\mathbf{q},\lambda)\left(b_{\mathbf{q}\lambda} + b^\dagger_{\mathbf{q}\lambda}\right) e^{i\mathbf{q}\cdot\mathbf{R}_1}\rho_{1\mathbf{q}}, \tag{2.16}$$

$$H_{2e-\rm ph} = \sum_{\mathbf{q},\lambda} M_2(\mathbf{q},\lambda)\left(b_{\mathbf{q}\lambda} + b^\dagger_{\mathbf{q}\lambda}\right) e^{i\mathbf{q}\cdot\mathbf{R}_2}\rho_{2\mathbf{q}}, \tag{2.17}$$

in which

$$\rho_{1\mathbf{q}} = \sum_{\mathbf{k},\sigma}^{1} c^\dagger_{1,\mathbf{k}+\mathbf{q}\sigma}c_{1,\mathbf{k}\sigma}, \tag{2.18}$$

and

$$\rho_{2\mathbf{q}} = \sum_{\mathbf{k},\sigma}^{2} c^{\dagger}_{2,\mathbf{k}+\mathbf{q}\sigma} c_{2,\mathbf{k}\sigma}, \tag{2.19}$$

are density operators for type-1 and type-2 carriers, $u_i(\mathbf{q})$ and $M_i(\mathbf{q},\lambda)$ are intrasubband electron-impurity potentials and electron-phonon matrix elements for system i ($i = 1, 2$), and $b^{\dagger}_{\mathbf{q}\lambda}$ ($b_{\mathbf{q}\lambda}$) are creation (annihilation) operators for phonons with wave vector $\mathbf{q}$ and frequency $\Omega_{\mathbf{q}\lambda}$. The phonon part of the Hamiltonian is

$$H_{ph} = \sum_{\mathbf{q},\lambda} \Omega_{\mathbf{q}\lambda} b^{\dagger}_{\mathbf{q}\lambda} b_{\mathbf{q}\lambda}. \tag{2.20}$$

In Eq.(2.8) H_{12} stands for the Coulomb interaction between different types of carriers (intersubband Coulomb interaction):

$$H_{12} = \sum_{\mathbf{q}} V_{12}(q) e^{i\mathbf{q}\cdot(\mathbf{R}_1-\mathbf{R}_2)} \rho_{1\mathbf{q}} \rho_{2-\mathbf{q}}. \tag{2.21}$$

Finally, $H^{12}_{e-\mathrm{ph}}$ and $H^{21}_{e-\mathrm{ph}}$ are intersubband electron-phonon interactions:

$$H^{12}_{e-\mathrm{ph}} = \sum_{\mathbf{q},\lambda} M_{12}(\mathbf{q},\lambda) \left(b_{\mathbf{q}\lambda} + b^{\dagger}_{\mathbf{q}\lambda}\right) e^{i\mathbf{q}\cdot\mathbf{R}_1} \sum_{\mathbf{k},\sigma} e^{i\mathbf{q}\cdot(\mathbf{R}_1-\mathbf{R}_2)} c^{\dagger}_{1,\mathbf{k}+\mathbf{q}\sigma} c_{2,\mathbf{k}\sigma}, \tag{2.22}$$

$$H^{21}_{e-\mathrm{ph}} = \sum_{\mathbf{q},\lambda} M_{21}(\mathbf{q},\lambda) \left(b_{\mathbf{q}\lambda} + b^{\dagger}_{\mathbf{q}\lambda}\right) e^{i\mathbf{q}\cdot\mathbf{R}_2} \sum_{\mathbf{k},\sigma} e^{i\mathbf{q}\cdot(\mathbf{R}_2-\mathbf{R}_1)} c^{\dagger}_{2,\mathbf{k}+\mathbf{q}\sigma} c_{1,\mathbf{k}\sigma}, \tag{2.23}$$

with $M_{12}(\mathbf{q},\lambda) = M_{21}(\mathbf{q},\lambda)$ being matrix elements for intersubband electron-phonon scattering. Here, intersubband electron-impurity scatterings are neglected.

Basing on the Hamiltonian (2.8), one can determine the rates of changes of the center-of-mass momenta $\mathbf{P}_1$ and $\mathbf{P}_2$, the relative electron energies H_{1e} and H_{2e}, and the subsystem particle number N_1 from the general relation

$$\dot{O} = -i\,[O, H]. \tag{2.24}$$

The derivation of balance equations requires calculation of the statistical averager of the time derivatives of the related quantities with respect to the appropriate density matrix of the system. Here the Liouville equation for the statistical density matrix ρ of the relative electron-phonon system takes the form

$$i\frac{\partial \rho}{\partial t} = [H_{\mathrm{c.m.}T} + H_{1e} + H_{2e} + H_I, \rho]. \tag{2.25}$$

And the initial condition for the density matrix ρ is chosen as

$$\rho|_{t=-\infty} = \rho_0 = \frac{1}{Z_{ph}} e^{-H_{ph}/T} \frac{1}{Z_1} e^{-(H_{1e}-\mu_1 N_1)/T_{1e}} \frac{1}{Z_2} e^{-(H_{2e}-\mu_2 N_2)/T_{2e}}. \tag{2.26}$$

Therefore, using the Green's function method, balance equations for forces, energies, and particle numbers are derived for the steady state transport under a uniform electric field

$$N_1 e\mathbf{E} + \mathbf{F}_1(v_1) + \mathbf{F}^{12}_p(v_1, v_2) + \mathbf{F}_{12}(v_1 - v_2) = 0, \tag{2.27}$$

$$N_2 e\mathbf{E} + \mathbf{F}_2(v_2) + \mathbf{F}^{21}_p(v_1, v_2) - \mathbf{F}_{12}(v_1 - v_2) = 0, \tag{2.28}$$

$$\mathbf{v}_1 \cdot \mathbf{F}_1(v_1) + W_1(v_1) + W_p^{12}(v_1, v_2) + W_{12}(v_1 - v_2) = 0, \tag{2.29}$$

$$\mathbf{v}_2 \cdot \mathbf{F}_2(v_2) + (\mathbf{v}_1 - \mathbf{v}_2) \cdot \mathbf{F}_{12}(v_1 - v_2) + W_2(v_2) + W_p^{21}(v_1, v_2) - W_{12}(v_1 - v_2) = 0, \tag{2.30}$$

$$N(v_1, T_{1e}, \mu_1, v_2, T_{2e}, \mu_2) = 0. \tag{2.31}$$

Here $\mathbf{v}_1$ and $\mathbf{v}_2$ are the average drift velocities, T_{1e} and T_{2e} are the electron temperatures, N_1, μ_1 and N_2 μ_2 are theparticle numbers chemical potentials of the type-1 and type-2 carriers respectively. $\mathbf{F}_1$, $\mathbf{F}_2$, W_1 and W_2 denote the frictional forces and energy-loss rates for carrier systems 1 and 2 due to intra-system interaction. $\mathbf{F}_{12}$ and W_{12} are the force experienced by the center of mass and the energy-loss rate of carrier system 1 due to inter-system Coulomb interaction. $\mathbf{F}_p^{12}$ and W_p^{12} or $\mathbf{F}_p^{21}$ and W_p^{21} represent the frictional force and energy-loss rate of the carrier system 1 or 2 due to iner-system electron-phonon interactions, respectively. Finally, N is the rate of changes of the particle number of the carrier system 1 due to inter-system electron-phonon couplings. Eqs.(2.27)~(2.31), together with the constraint

$$N_1 + N_2 = N \tag{2.32}$$

and the relations

$$N_i = \sum_{\mathbf{k}\sigma} f\left(\left(\varepsilon_{i\mathbf{k}} - \mu_i\right)/T_{ie}\right) \qquad (i = 1, 2) \tag{2.33}$$

($f(x) = 1/(\exp(x) + 1)$ represents the Fermi-Dirac distribution function) form a complete set of equations to determine the steady-state values of v_1, v_2, T_{1e}, T_{2e}, μ_1, μ_2 for given electric field $\mathbf{E}$, lattice temperature T and total electron density N.

In the limit of weak applied electric field strength, the balance equations (2.27)-(2.31) can be expanded to linear order in the carrier-drift velocites. In this situation the energy-balance equations (2.29) and (2.30) and the particle number equation (2.31) mandate that $T_{1e} = T_{2e} = T$ and $\mu_1 = \mu_2$, while the momentum-force balance equations (2.27) and (2.28) take the form along the electric field direction

$$N_1 eE + v_1 F_1' + v_1 \left[F_p^{12}\right]_1' + v_2 \left[F_p^{12}\right]_2' + (v_1 - v_2) F_{12}' = 0, \tag{2.34}$$

$$N_2 eE + v_2 F_2' + v_2 \left[F_p^{21}\right]_2' + v_1 \left[F_p^{21}\right]_1' - (v_1 - v_2) F_{12}' = 0, \tag{2.35}$$

where $F_i' = (\partial/\partial v_i)\, F_i(v_i)|_{v_i=0}$, $\left[F_p^{ij}\right]_i' = (\partial/\partial v_i)\, F_p^{ij}(v_i, v_j)|_{v_i=v_j=0}$ and $F_{12}' = (\partial/\partial(v_1 - v_2))\, F_{12}(v_1 - v_2)|_{v_1-v_2=0}$ $(i, j = 1, 2)$. The drift velocities v_1 and v_2 can be obtained by straightly solving this group of linear equations (2.34) and (2.35). The total drift velocity v of the system is defined as

$$v = \frac{N_1 v_1 + N_2 v_2}{N}, \tag{2.36}$$

and the total mobility is obtained

$$\mu = \frac{v}{E}. \tag{2.37}$$

2.3 Electron Transport in Quantum Wells

Consider a GaAs quantum-well of width d embedded in $Al_xGa_{1-x}As$ as a model quasi-two-dimensional systems. Assuming infinitely deep wells, we can write the electron wave functions and energies as:

$$\psi^{2D}_{n\mathbf{k}} = \frac{1}{S^{1/2}}\zeta_n(z)e^{i\mathbf{k}\cdot\mathbf{r}_\parallel},$$

$$\varepsilon_{n\mathbf{k}} = \varepsilon_n + \frac{\hbar^2 k^2}{2m^*},$$

where $\varepsilon_n(=\frac{\pi^2\hbar^2 n^2}{2m^* d^2})$ is the nth subband energy due to the quantized motion in the z direction and m^* the electron effective mass, S is the area of the 2D plane, $\mathbf{k} = (k_x, k_y)$ the two-dimensional plane wave vector and $\mathbf{r}_\parallel = (x, y)$ the 2D coordinate. $\zeta_n(z)$ denotes the nth subband envelope wave function. For the lowest two subbands we have

$$\begin{aligned} \zeta_0(z) &= \sqrt{\frac{2}{d}}\sin\left(\frac{\pi z}{d}\right), \\ \zeta_1(z) &= \sqrt{\frac{2}{d}}\sin\left(\frac{2\pi z}{d}\right). \end{aligned} \tag{2.38}$$

In second quantization representation the system can be described by the following Hamiltonian:

$$H_e = \sum_{n\mathbf{k}\sigma} \varepsilon_{n\mathbf{k}\sigma} c^\dagger_{n\mathbf{k}\sigma} c_{n\mathbf{k}\sigma} + \frac{1}{2}\sum_{\substack{m',m,n',n \\ \mathbf{k},\mathbf{k}_1,\mathbf{q} \\ \sigma,\sigma_1}} V_{m'm,n'n}(q) c^\dagger_{m'\mathbf{k}+\mathbf{q}\sigma} c^\dagger_{n'\mathbf{k}_1-\mathbf{q}-\sigma} c_{n\mathbf{k}_1\sigma_1} c_{m\mathbf{k}\sigma} \tag{2.39}$$

with

$$V_{m'm,n'n}(q) = \frac{e^2}{2\epsilon_0\kappa q} H_{m'm,n'n}(q), \tag{2.40}$$

$$H_{m'm,n'n}(q) = \int dz_1 dz_2 \zeta^*_{m'}(z_1)\zeta_m(z_1)\zeta^*_{n'}(z_2)\zeta_n(z_2)e^{-q|z_1-z_2|} \tag{2.41}$$

where κ is the dielectric constant of GaAs; $\mathbf{q} = (q_x, q_y)$. $H_{m'm,n'n}$ is the form factors of the electron-electron Coulomb interactions $V_{m'm,n'n}$ describing the collision between an electron in subband n and an electron in subband m, which are scattered into subband n' and subband m', respectively. They can be divided into three classes. The first class terms, $V_{00,00}$ and $V_{11,11}$, are the intrasubband Coulomb interactions of subbands 0 and 1. The second class terms, $V_{00,11}$ and $V_{11,00}$ ($V_{00,11} = V_{11,00}$), describe the behavior of the intersubband Coulomb scattering but no exchanging of electrons between different subbands. All other terms constitute the third class, which involve exchanging and transferring of electrons between the two subbands. Due to the orthogonality of the wave functions, the third class terms are small, as can be seen in Fig.2-1, where the square of form factors $|H_{m'm,n'n}(q)|^2$ are plotted as function of q. The thick lines represent the square of the former two classes Coulomb form factors and thin lines correspond to those of the third class. The square of form factors of the third class are at least one order of magnitude smaller than those of other two classes (here $H_{00,01}$ and $H_{01,11} = 0$). Therefore, we consider only the first and second classes Coulomb interactions in our present calculation. The intrasubband interactions $V_{00,00}$ and $V_{11,11}$ are assumed strong enough to establish a unique electron temperature within each subband, and their further roles are treated through the dynamical screening. Our main interest is focused on the effect of the intersubband interactions $V_{00,11}$ and $V_{11,00}$ on hot-electron transport properties. We will see that it is these terms that make each subband of the system approach a common electron temperature although we assume

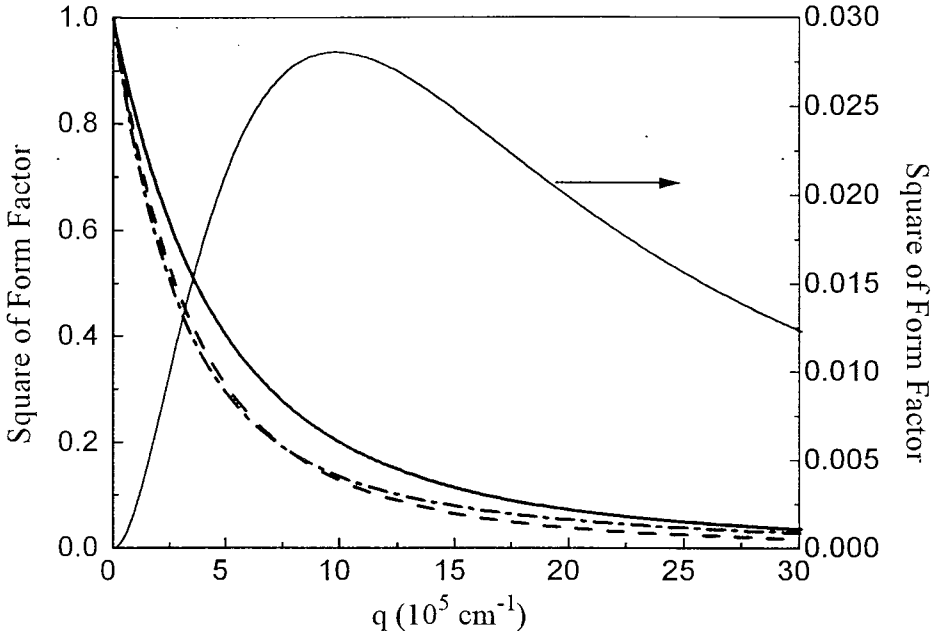

Figure 2-1: Form factors of e-e Coulomb interactions for $Al_xGa_{1-x}As$-GaAs quasi-2D quantum-well with width 50 nm versus the plane wave vector q are plotted. The thick solid line stands for $|H_{00,00}(q)|^2$, the dashed line for $|H_{11,11}(q)|^2$ and the dotted-dashed line for $|H_{00,11}(q)|^2$. Thin solid curves denote form factors of the third class of the e-e Coulomb interactions.

that different subbands possess different electron temperatures within the theoretical framework when the electron.density is enough high.

Basing on this approximation, the Hamiltionian of the system can be rewritten, approximately, by

$$H_e = H_{0e} + H_{1e} + H_{01}. \tag{2.42}$$

$$H_{0e} = \sum_{0\mathbf{k}\sigma} \varepsilon_{0\mathbf{k}\sigma} c^\dagger_{0\mathbf{k}\sigma} c_{0\mathbf{k}\sigma} + \frac{1}{2} \sum_{\substack{\mathbf{k},\mathbf{k}_1,\mathbf{q} \\ \sigma,\sigma_1}} V_{00,00}(q) c^\dagger_{0\mathbf{k}+\mathbf{q}\sigma} c^\dagger_{0\mathbf{k}_1-\mathbf{q}-\sigma} c_{0\mathbf{k}_1\sigma_1} c_{0\mathbf{k}\sigma}, \tag{2.43}$$

$$H_{1e} = \sum_{1\mathbf{k}\sigma} \varepsilon_{1\mathbf{k}\sigma} c^\dagger_{1\mathbf{k}\sigma} c_{1\mathbf{k}\sigma} + \frac{1}{2} \sum_{\substack{\mathbf{k},\mathbf{k}_1,\mathbf{q} \\ \sigma,\sigma_1}} V_{11,11}(q) c^\dagger_{1\mathbf{k}+\mathbf{q}\sigma} c^\dagger_{1\mathbf{k}_1-\mathbf{q}-\sigma} c_{1\mathbf{k}_1\sigma_1} c_{1\mathbf{k}\sigma}, \tag{2.44}$$

$$\begin{aligned} H_{01} &= \frac{1}{2} \sum_{\substack{\mathbf{k}\mathbf{k}'\mathbf{q} \\ \sigma\sigma'}} V_{00,11}(q) e^{i\mathbf{q}\cdot(\mathbf{R}_0-\mathbf{R}_1)} c^\dagger_{0\mathbf{k}+\mathbf{q}\sigma} c^\dagger_{1\mathbf{k}'-\mathbf{q}\sigma'} c_{1\mathbf{k}'\sigma'} c_{0\mathbf{k}\sigma} \\ &+ \frac{1}{2} \sum_{\substack{\mathbf{k}\mathbf{k}'\mathbf{q} \\ \sigma\sigma'}} V_{11,00}(q) e^{i\mathbf{q}\cdot(\mathbf{R}_1-\mathbf{R}_0)} c^\dagger_{1\mathbf{k}+\mathbf{q}\sigma} c^\dagger_{0\mathbf{k}'-\mathbf{q}\sigma'} c_{0\mathbf{k}'\sigma'} c_{1\mathbf{k}\sigma}. \end{aligned} \tag{2.45}$$

Further, we can rewrite it in terms of density operator:

$$\begin{aligned} H_{01} &= \frac{1}{2} \sum_{\mathbf{q}} V_{00,11}(q) e^{i\mathbf{q}\cdot(\mathbf{R}_0-\mathbf{R}_1)} \rho_{0\mathbf{q}} \rho_{1-\mathbf{q}} + \frac{1}{2} \sum_{\mathbf{q}} V_{11,00}(q) e^{i\mathbf{q}\cdot(\mathbf{R}_1-\mathbf{R}_0)} \rho_{1\mathbf{q}} \rho_{0-\mathbf{q}} \\ &= \sum_{\mathbf{q}} V_{00,11}(q) e^{i\mathbf{q}\cdot(\mathbf{R}_0-\mathbf{R}_1)} \rho_{0\mathbf{q}} \rho_{1-\mathbf{q}}. \end{aligned} \tag{2.46}$$

Now, according to the treatment of above section, in the presence of a uniform electric field $\mathbf{E}$ parallel to the interface of the quantum well, we can treat electrons dwelling in the ground subband and the first excited subband as two different types of carriers. It is natural that, due to the enough strong intrasubband Coulomb interactions, we can assume electrons within each subband having unique averaged drift velocities, electron temperatures and chemical potentials. So the total Hamiltonian of the system can be written as:

$$\begin{aligned} H &= H_{c.m.E} + H_{c.m.T} + H_{0e} + H_{1e} + H_{ph} + H_I, \\ H_I &= H_{01} + H^{00}_{e-i} + H^{11}_{e-i} + H^{01}_{e-i} + H^{10}_{e-i} + H^{00}_{e-ph} + H^{11}_{e-ph} + H^{01}_{e-ph} + H^{10}_{e-ph}. \end{aligned} \tag{2.47}$$

where

$$H^{n'n}_{e-i} = \sum_{\mathbf{k},\mathbf{q},a,\sigma} U_{n'n}(q,z_a) e^{i\mathbf{q}\cdot(\mathbf{R}-\mathbf{r}_a)} c^{\dagger}_{n'\mathbf{k}+\mathbf{q}\sigma} c_{n\mathbf{k}\sigma}, \tag{2.48}$$

$$H^{n'n}_{e-ph} = \sum_{\mathbf{q},q_z,\lambda} M_{n'n}(\mathbf{q},q_z,\lambda) e^{i\mathbf{q}\cdot\mathbf{R}} \left(b_{\mathbf{Q}\lambda} + b^{\dagger}_{-\mathbf{Q}\lambda}\right) \sum_{\mathbf{k},\sigma} c^{\dagger}_{n'\mathbf{k}+\mathbf{q}\sigma} c_{n\mathbf{k}\sigma}, \tag{2.49}$$

with $U_{n'n}(q,z_a) = \frac{2\pi Z e^2}{\kappa q} F_{n'n}(q,z_a)$ and $M_{n'n}(\mathbf{q},q_z,\lambda) = M(\mathbf{q},q_z,\lambda) I^*_{n'n}(iq_z)$,

$$F_{n'n}(q,z_a) = \int_0^{\infty} e^{-q|z-z_a|} \zeta^*_{n'}(z)\zeta_n(z)dz, \tag{2.50}$$

$$I_{n'n} = \int_0^{\infty} e^{-iq_z z} \zeta^*_{n'}(z)\zeta_n(z)dz. \tag{2.51}$$

Thus the same procedure as above section leads to the force, energy, and particle number balance equations, in a steady-transport state. In the quasi-2D systems the frictional forces and energy-loss rates of electrons within the subband i are given by

$$\begin{aligned} \mathbf{F}^{2D}_i &= n_i \sum_{\mathbf{q}} |u_{ii}(\mathbf{q})|^2 \mathbf{q} \Pi^{(i)}_2(\mathbf{q},\omega_i) + \\ &\quad 2 \sum_{\mathbf{q},q_z,\lambda} |M_{ii}(\mathbf{Q},\lambda)|^2 \mathbf{q} \Pi^{(i)}_2(\mathbf{q},\omega_i + \Omega_{\mathbf{Q}\lambda}) \left[n\left[\frac{\Omega_{\mathbf{Q}\lambda}}{T}\right] - n\left[\frac{\omega_i + \Omega_{\mathbf{Q}\lambda}}{T_{ie}}\right]\right], \\ W^{2D}_i &= 2 \sum_{\mathbf{q},q_z,\lambda} |M_{ii}(\mathbf{Q},\lambda)|^2 \Omega_{\mathbf{Q}\lambda} \Pi^{(i)}_2(\mathbf{q},\omega_i + \Omega_{\mathbf{Q}\lambda}) \left[n\left[\frac{\Omega_{\mathbf{Q}\lambda}}{T}\right] - n\left[\frac{\omega_i + \Omega_{\mathbf{Q}\lambda}}{T_{ie}}\right]\right], \end{aligned} \tag{2.52}$$

with $\omega_i \equiv \mathbf{q}\cdot\mathbf{v}_i (i = 0,1)$. The force and energy-loss rate of electrons within subband 0 due to inter-subband Coulomb interaction are

$$\begin{aligned} \mathbf{F}^{2D}_{01} &= \sum_{\mathbf{q}} |V_{00,11}(\mathbf{q})|^2 \mathbf{q} \int_{-\infty}^{\infty} \frac{d\omega}{\pi} \left[n\left[\frac{\omega}{T_{0e}}\right] - n\left[\frac{\omega-\omega_{01}}{T_{1e}}\right]\right] \Pi^{(0)}_2(\mathbf{q},\omega)\Pi^{(1)}_2(\mathbf{q},\omega-\omega_{01}), \\ W^{2D}_{01} &= \sum_{\mathbf{q}} |V_{00,11}(\mathbf{q})|^2 \int_{-\infty}^{\infty} \frac{d\omega}{\pi} \omega \left[n\left[\frac{\omega}{T_{0e}}\right] - n\left[\frac{\omega-\omega_{01}}{T_{1e}}\right]\right] \Pi^{(0)}_2(\mathbf{q},\omega)\Pi^{(1)}_2(\mathbf{q},\omega-\omega_{01}), \end{aligned} \tag{2.53}$$

with $\omega_{01} \equiv \mathbf{q}\cdot(\mathbf{v}_0 - \mathbf{v}_1)$,

In these equations $\Pi^{(i)}_2(\mathbf{q},\omega)$ and $\Pi^{(i)}_2(q_z,\omega)$ are the imaginary parts of the electron density-density correlation functions of the subband i at temperature T_{ie} for quasi-2D systems. Under random-phase approximation the density-density correlation functions can be written as

$$\Pi^{(i)}(\mathbf{q},\omega) = \frac{\pi^{(i)}(\mathbf{q},\omega)}{1 - V_{ii,ii}(q)\pi^{(i)}(\mathbf{q},\omega)}. \tag{2.54}$$

in which

$$\pi^{(i)} = 2\sum_{\mathbf{k}} \frac{f\left((\varepsilon_{i\mathbf{k}+\mathbf{q}} - \mu_i)/T_{ie}\right) - f\left((\varepsilon_{i\mathbf{k}} - \mu_i)/T_{ie}\right)}{\omega + \varepsilon_{i\mathbf{k}+\mathbf{q}} - \varepsilon_{i\mathbf{k}} + i\delta} \tag{2.55}$$

are the density-density correlation functions of the carrier systems in the absence of intra-subband Coulomb interaction. $n(x)$ is the Bose distribution function ($n(x) = 1/(\exp(x) - 1)$).

The friction force experienced by electrons within the subband 0 and the energy-loss rate of electron of the same subband due to inter-subband electron-phonon interaction are

$$\begin{aligned}
\mathbf{F}^{01}_{p,2D} = & -4\pi \sum_{\mathbf{k},\mathbf{q},q_z,\lambda} |M_{01}(\mathbf{Q},\lambda)|^2 \, \mathbf{k} \left[f\left(\xi_{0\mathbf{k}}/T_{0e}\right) - f\left(\xi_{1\mathbf{k}+\mathbf{q}}/T_{1e}\right)\right] \\
& \times \left\{ \left[n\left[\frac{\Omega_{\mathbf{Q}\lambda}}{T}\right] - n\left[\frac{\xi_{0\mathbf{k}}}{T_{0e}} - \frac{\xi_{1\mathbf{k}+\mathbf{q}}}{T_{1e}}\right] \right] \delta\left(E_{1\mathbf{k}+\mathbf{q}} - E_{0\mathbf{k}} + \Omega_{\mathbf{Q}\lambda}\right) \right. \\
& \left. + \left[n\left[\frac{\Omega_{\mathbf{Q}\lambda}}{T}\right] - n\left[\frac{\xi_{1\mathbf{k}+\mathbf{q}}}{T_{1e}} - \frac{\xi_{0\mathbf{k}}}{T_{0e}}\right] \right] \delta\left(E_{1\mathbf{k}+\mathbf{q}} - E_{0\mathbf{k}} - \Omega_{\mathbf{Q}\lambda}\right) \right\},
\end{aligned} \tag{2.56}$$

$$\begin{aligned}
W^{01}_{p,2D} = & \; 4\pi \sum_{\mathbf{k},\mathbf{q},q_z,\lambda} |M_{01}(\mathbf{Q},\lambda)|^2 \, \varepsilon_{0\mathbf{k}} \left[f\left(\xi_{0\mathbf{k}}/T_{0e}\right) - f\left(\xi_{1\mathbf{k}+\mathbf{q}}/T_{1e}\right)\right] \\
& \times \left\{ \left[n\left[\frac{\Omega_{\mathbf{Q}\lambda}}{T}\right] - n\left[\frac{\xi_{0\mathbf{k}}}{T_{0e}} - \frac{\xi_{1\mathbf{k}+\mathbf{q}}}{T_{1e}}\right] \right] \delta\left(E_{1\mathbf{k}+\mathbf{q}} - E_{0\mathbf{k}} + \Omega_{\mathbf{Q}\lambda}\right) \right. \\
& \left. + \left[n\left[\frac{\Omega_{\mathbf{Q}\lambda}}{T}\right] - n\left[\frac{\xi_{1\mathbf{k}+\mathbf{q}}}{T_{1e}} - \frac{\xi_{0\mathbf{k}}}{T_{0e}}\right] \right] \delta\left(E_{1\mathbf{k}+\mathbf{q}} - E_{0\mathbf{k}} - \Omega_{\mathbf{Q}\lambda}\right) \right\},
\end{aligned} \tag{2.57}$$

in which $\xi_{i\mathbf{k}} = E_{i\mathbf{k}} - \mu_i$, $E_{i\mathbf{k}} = \varepsilon_{i\mathbf{k}} + \frac{1}{2}m^* v_i^2 + \mathbf{k}\cdot\mathbf{v}_i$,

The expressions for F_p^{10} and W_p^{10} can be obtained from Eqs.(2.56), (2.57) by exchanging all the indices $0 \rightleftharpoons 1$, respectively.

Finally, the rate of change of the particle number of the electrons within the subband 0 is due to inter-subband electron-phonon coupling:

$$\begin{aligned}
N^{2D} = & -4\pi \sum_{\mathbf{k},\mathbf{q},q_z,\lambda} |M_{01}(\mathbf{Q},\lambda)|^2 \left[f\left(\xi_{0\mathbf{k}}/T_{0e}\right) - f\left(\xi_{1\mathbf{k}+\mathbf{q}}/T_{1e}\right)\right] \\
& \times \left\{ \left[n\left[\frac{\Omega_{\mathbf{Q}\lambda}}{T}\right] - n\left[\frac{\xi_{0\mathbf{k}}}{T_{0e}} - \frac{\xi_{1\mathbf{k}+\mathbf{q}}}{T_{1e}}\right] \right] \delta\left(E_{1\mathbf{k}+\mathbf{q}} - E_{0\mathbf{k}} + \Omega_{\mathbf{Q}\lambda}\right) \right. \\
& \left. + \left[n\left[\frac{\Omega_{\mathbf{Q}\lambda}}{T}\right] - n\left[\frac{\xi_{1\mathbf{k}+\mathbf{q}}}{T_{1e}} - \frac{\xi_{0\mathbf{k}}}{T_{0e}}\right] \right] \delta\left(E_{1\mathbf{k}+\mathbf{q}} - E_{0\mathbf{k}} - \Omega_{\mathbf{Q}\lambda}\right) \right\},
\end{aligned} \tag{2.58}$$

2.4 Electron Transport in Quantum Wires

We choose a cylinder GaAs quantum wire of radius ρ embedded in $Al_xGa_{1-x}As$ as model quasi-1D system. The wave function and the energy of the quantum wire of length L_z are

$$\psi^{1D}_{nmk_z} = \frac{1}{L_z^{1/2}} e^{ik_z z} \zeta_{nm}(z),$$

$$\varepsilon_{nmk_z} = \frac{k_z^2}{2m^*} + \varepsilon_{nm}.$$

$\zeta_{nm}(z)$ is the envelope wave functions and ε_{nm} is the subband energy due to the confinement. In the following, we consider only the ground subband $n = 0$, $m = 1$ and next two degenerate subbands:

$n = 1$, $m = 1$ and $n = -1$, $m = 1$, having wave functions and eigenenergies

$$\begin{aligned} \zeta_{01}(\mathbf{r}_\parallel) &= C_1^0 J_0\left(\frac{x_1^0}{\rho} r_\parallel\right), \\ \zeta_{\pm 11}(\mathbf{r}_\parallel) &= \pm C_1^{\pm 1} J_1\left(\frac{x_1^1}{\rho} r_\parallel\right) e^{\pm i\phi}, \end{aligned} \tag{2.59}$$

$$\varepsilon_{nm} = \frac{\left(x_m^{|n|}\right)^2}{2m^*\rho^2}, \tag{2.60}$$

where $C_m^n = 1/(\sqrt{\pi} y_m^n \rho)$ is the normalization factor, $x_m^{|n|}$ is the mth zero of the nth-order Bessel function, i.e. $J_n(x_{|n|}) = 0$ and $y_m^n = J_{|n|+1}(x_m^{|n|})$. The difference from the quasi-2D systems is that the $n = 1$ subband has a degenerate one $n = -1$. Since $m = 1$ for these three subbands, we omit this subscript for simplicity. In the framework of balance-equation approach of TTCM, the two degenerate subbands share a unique electron temperature, drift velocity and Fermi energy which may be different from those of the subband $n = 0$. The electron Hamiltonian reads

$$H_e = \sum_{nk_z\sigma} \varepsilon_{nk_z\sigma} c^\dagger_{nk_z\sigma} c_{nk_z\sigma} + \frac{1}{2} \sum_{\substack{m',m,n',n \\ k_z,k_z',q_z \\ \sigma,\sigma'}} K_{m'm,n'n}(|q_z|) c^\dagger_{m'k_z+q_z\sigma} c^\dagger_{n'k_z'-q_z-\sigma'} c_{nk_z'\sigma'} c_{mk_z\sigma}, \tag{2.61}$$

where

$$K_{m'm,n'n}(|q_z|) = \frac{e^2}{4\pi\epsilon_0\kappa} \int d\mathbf{r}_\parallel d\mathbf{r}_\parallel' \zeta^*_{m'}(\mathbf{r}_\parallel)\zeta_m(\mathbf{r}_\parallel)\zeta^*_{n'}(\mathbf{r}_\parallel')\zeta_n(\mathbf{r}_\parallel') K_0(|q_z||\mathbf{r}_\parallel - \mathbf{r}_\parallel'|) \tag{2.62}$$

is the Coulomb interaction. $K_0(x)$ is the modified Bessel function of zeroth order. As in the case of the quasi-2D systems, the inter-subband Coulomb scatterings $K_{00,11}(= K_{00,\bar{1}\bar{1}})$ are our main concern terms (see Fig.2-2). The equations of force, energy, and particle number balance in quantum wire system under a uniform electric field $\mathbf{E}$ along the z-direction are as follows:

$$N_0 e\mathbf{E} + \mathbf{F}_0(v_0) + 2\mathbf{F}_p^{01}(v_0, v_1) + 2\mathbf{F}_{01}(v_0 - v_1) = 0, \tag{2.63}$$

$$2N_1 e\mathbf{E} + 2\mathbf{F}_1(v_1) + 2\mathbf{F}_p^{10}(v_0, v_1) - 2\mathbf{F}_{01}(v_0 - v_1) = 0, \tag{2.64}$$

$$\mathbf{v}_0 \cdot \mathbf{F}_0(v_0) + W_0(v_0) + 2W_p^{01}(v_0, v_1) + 2W_{01}(v_0 - v_1) = 0, \tag{2.65}$$

$$\mathbf{v}_1 \cdot 2\mathbf{F}_1(v_1) + (\mathbf{v}_0 - \mathbf{v}_1) \cdot 2\mathbf{F}_{01}(v_0 - v_1) + 2W_1(v_1) + 2W_p^{10}(v_0, v_1) - 2W_{01}(v_0 - v_1) = 0, \tag{2.66}$$

$$X(v_0, T_{0e}, \mu_0, v_1, T_{1e}, \mu_1) = 0. \tag{2.67}$$

and

$$N_0 + 2N_1 = N \tag{2.68}$$

Here, $\mathbf{F}$, W and X functions have the same meaning as those of above section. The frictional forces and energy-loss rates of electrons within the subband i are given, respectively, as:

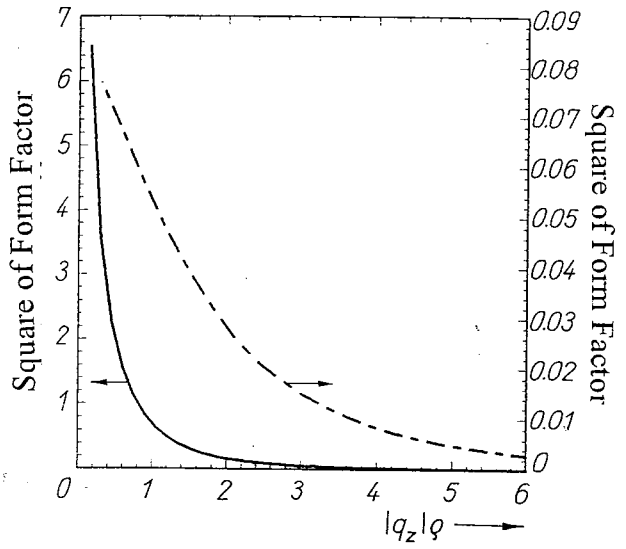

Figure 2-2: Form factors of e-e Coulomb interactions for $Al_xGa_{1-x}As$-GaAs quasi-1D quantum-wire with radius 9 nm versus the plane wave vector $|q_z|\rho$ are plotted. The solid line stands for $|H_{00,11}(q)|^2$. The dotted-dashed curve denotes form factors of the third class of the e-e Coulomb interactions.

$$
\begin{aligned}
F_i^{1D} &= n_i \sum_{\mathbf{q},q_z} |u_{ii}(\mathbf{Q})|^2 q_z \Pi_2^{(i)}(q_z, q_z v_i) + \\
&\quad 2 \sum_{\mathbf{q},q_z,\lambda} |M_{ii}(\mathbf{Q},\lambda)|^2 \, q_z \Pi_2^{(i)}(q_z, q_z v_i + \Omega_{\mathbf{Q}\lambda}) \left[n\left[\frac{\Omega_{\mathbf{Q}\lambda}}{T}\right] - n\left[\frac{q_z v_i + \Omega_{\mathbf{Q}\lambda}}{T_{ie}}\right]\right], \qquad (2.69) \\
W_i^{1D} &= 2 \sum_{\mathbf{q},q_z,\lambda} |M_{ii}(\mathbf{Q},\lambda)|^2 \, \Omega_{\mathbf{Q}\lambda} \Pi_2^{(i)}(q_z, q_z v_i + \Omega_{\mathbf{Q}\lambda}) \left[n\left[\frac{\Omega_{\mathbf{Q}\lambda}}{T}\right] - n\left[\frac{q_z v_i + \Omega_{\mathbf{Q}\lambda}}{T_{ie}}\right]\right].
\end{aligned}
$$

The force and energy-loss rate of electrons within subband 0 due to inter-subband Coulomb interaction are

$$
\begin{aligned}
F_{01}^{1D} &= \sum_{q_z} |K_{00,11}(|q_z|)|^2 \, q_z \int_{-\infty}^{\infty} \frac{d\omega}{\pi} \left[n\left[\frac{\omega}{T_{0e}}\right] - n\left[\frac{\omega-\omega_{01}}{T_{1e}}\right]\right] \Pi_2^{(0)}(q_z,\omega)\Pi_2^{(1)}(q_z,\omega-\omega_{01}), \\
W_{01}^{1D} &= \sum_{q_z} |K_{00,11}(|q_z|)|^2 \int_{-\infty}^{\infty} \frac{d\omega}{\pi} \omega \left[n\left[\frac{\omega}{T_{0e}}\right] - n\left[\frac{\omega-\omega_{01}}{T_{1e}}\right]\right] \Pi_2^{(0)}(q_z,\omega)\Pi_2^{(1)}(q_z,\omega-\omega_{01}),
\end{aligned} \qquad (2.70)
$$

with $\omega_{01} = q_z(v_0 - v_1)$.

In Eqs.(2.69), (2.70) $\Pi_2^{(i)}(q_z,\omega)$ are the imaginary parts of the electron density-density correlation functions of the subband i at temperature T_{ie} for quasi-1D systems.

The friction force experienced by electrons within the subband 0 and the energy-loss rate of electron of the same subband due to inter-subband electron-phonon interaction are

$$
\begin{aligned}
F^{01}_{p,1D} = & -4\pi \sum_{k_z,\mathbf{Q},q_z,\lambda} |M_{01}(\mathbf{Q},\lambda)|^2 k_z \left[f\left(\xi_{0k_z}/T_{0e}\right) - f\left(\xi_{1k_z+q_z}/T_{1e}\right)\right] \\
& \times \left\{ \left[n\left[\frac{\Omega_{\mathbf{Q}\lambda}}{T}\right] - n\left[\frac{\xi_{0k_z}}{T_{0e}} - \frac{\xi_{1k_z+q_z}}{T_{1e}}\right]\right] \delta\left(E_{1k_z+q_z} - E_{0k_z} + \Omega_{\mathbf{Q}\lambda}\right) \right. \\
& \left. + \left[n\left[\frac{\Omega_{\mathbf{Q}\lambda}}{T}\right] - n\left[\frac{\xi_{1k_z+q_z}}{T_{1e}} - \frac{\xi_{0k_z}}{T_{0e}}\right]\right] \delta\left(E_{1k_z+q_z} - E_{0k_z} - \Omega_{\mathbf{Q}\lambda}\right) \right\},
\end{aligned} \tag{2.71}
$$

$$
\begin{aligned}
W^{01}_{p,1D} = & \ 4\pi \sum_{k_z,\mathbf{Q},q_z,\lambda} |M_{01}(\mathbf{Q},\lambda)|^2 \varepsilon_{0k_z} \left[f\left(\xi_{0k_z}/T_{0e}\right) - f\left(\xi_{1k_z+q_z}/T_{1e}\right)\right] \\
& \times \left\{ \left[n\left[\frac{\Omega_{\mathbf{Q}\lambda}}{T}\right] - n\left[\frac{\xi_{0k_z}}{T_{0e}} - \frac{\xi_{1k_z+q_z}}{T_{1e}}\right]\right] \delta\left(E_{1k_z+q_z} - E_{0k_z} + \Omega_{\mathbf{Q}\lambda}\right) \right. \\
& \left. + \left[n\left[\frac{\Omega_{\mathbf{Q}\lambda}}{T}\right] - n\left[\frac{\xi_{1k_z+q_z}}{T_{1e}} - \frac{\xi_{0k_z}}{T_{0e}}\right]\right] \delta\left(E_{1k_z+q_z} - E_{0k_z} - \Omega_{\mathbf{Q}\lambda}\right) \right\}.
\end{aligned} \tag{2.72}
$$

in which $\xi_{i\mathbf{k}} = E_{i\mathbf{k}} - \mu_i$, $E_{i\mathbf{k}} = \varepsilon_{i\mathbf{k}} + \frac{1}{2}m^* v_i^2 + \mathbf{k}\cdot\mathbf{v}_i$.

The expressions for $F^{10}_{p,1D}$ and $W^{10}_{p,1D}$ can be obtained from Eqs.(2.71), (2.72) by exchanging all the indices $0 \rightleftharpoons 1$, respectively.

Finally, the rate of change of the particle number of the electrons within the subband 0 is due to inter-subband electron-phonon coupling:

$$
\begin{aligned}
N^{1D} = & -4\pi \sum_{k_z,\mathbf{Q},q_z,\lambda} |M_{01}(\mathbf{Q},\lambda)|^2 \left[f\left(\xi_{0k_z}/T_{0e}\right) - f\left(\xi_{1k_z+q_z}/T_{1e}\right)\right] \\
& \times \left\{ \left[n\left[\frac{\Omega_{\mathbf{Q}\lambda}}{T}\right] - n\left[\frac{\xi_{0k_z}}{T_{0e}} - \frac{\xi_{1k_z+q_z}}{T_{1e}}\right]\right] \delta\left(E_{1k_z+q_z} - E_{0k_z} + \Omega_{\mathbf{Q}\lambda}\right) \right. \\
& \left. + \left[n\left[\frac{\Omega_{\mathbf{Q}\lambda}}{T}\right] - n\left[\frac{\xi_{1k_z+q_z}}{T_{1e}} - \frac{\xi_{0k_z}}{T_{0e}}\right]\right] \delta\left(E_{1k_z+q_z} - E_{0k_z} - \Omega_{\mathbf{Q}\lambda}\right) \right\}.
\end{aligned} \tag{2.73}
$$

2.5 Discussion

Just as we mentioned in the first section, the intersubband scatterings, mainly attributed to the electron-electron Coulomb interactions, which effectively transfer energy between different subbands and thermalize electron dwelling in different subbands, depend strongly on the dimensionality of the system and the density of the carriers. So, in this section, detailed numerical calculations have been performed for GaAs-based quasi-2D quantum-well and quasi-1D quantum-wire systems with several different electron densities and confinement, quantum-well widths and quantum-wire radii, at lattice temperature $T = 80$ K. Contributions of electron-impurities scattering, intra- and inter-subband electron-phonon scatterings (including polar-optical-phonon, deformation potential and piezoelectric couplings) and the inter-subband Coulomb interaction are included in the calculations.

2.5.1 Dependence on Carrier Density

In Figs.2-3, we plot the calculated electron temperatures T_e and drift velocities v_0 and v_1 of two subbands as functions of the electric field for $Al_xGa_{1-x}As$-GaAs quantum well systems of a well width 50 nm having carrier sheet densities $N_s = 0.1$, 0.5, 1.0, 5.0 and 10×10^{11} cm^{-2}, respectively. The solid curves are the values of the ground subband 0, long-dashed curves are those of the first excited subband 1 and shot-dashed lines correspond to the average drift velocities v_d:

$$
v_d = \frac{N_0 v_0 + N_1 v_1}{N}.
$$

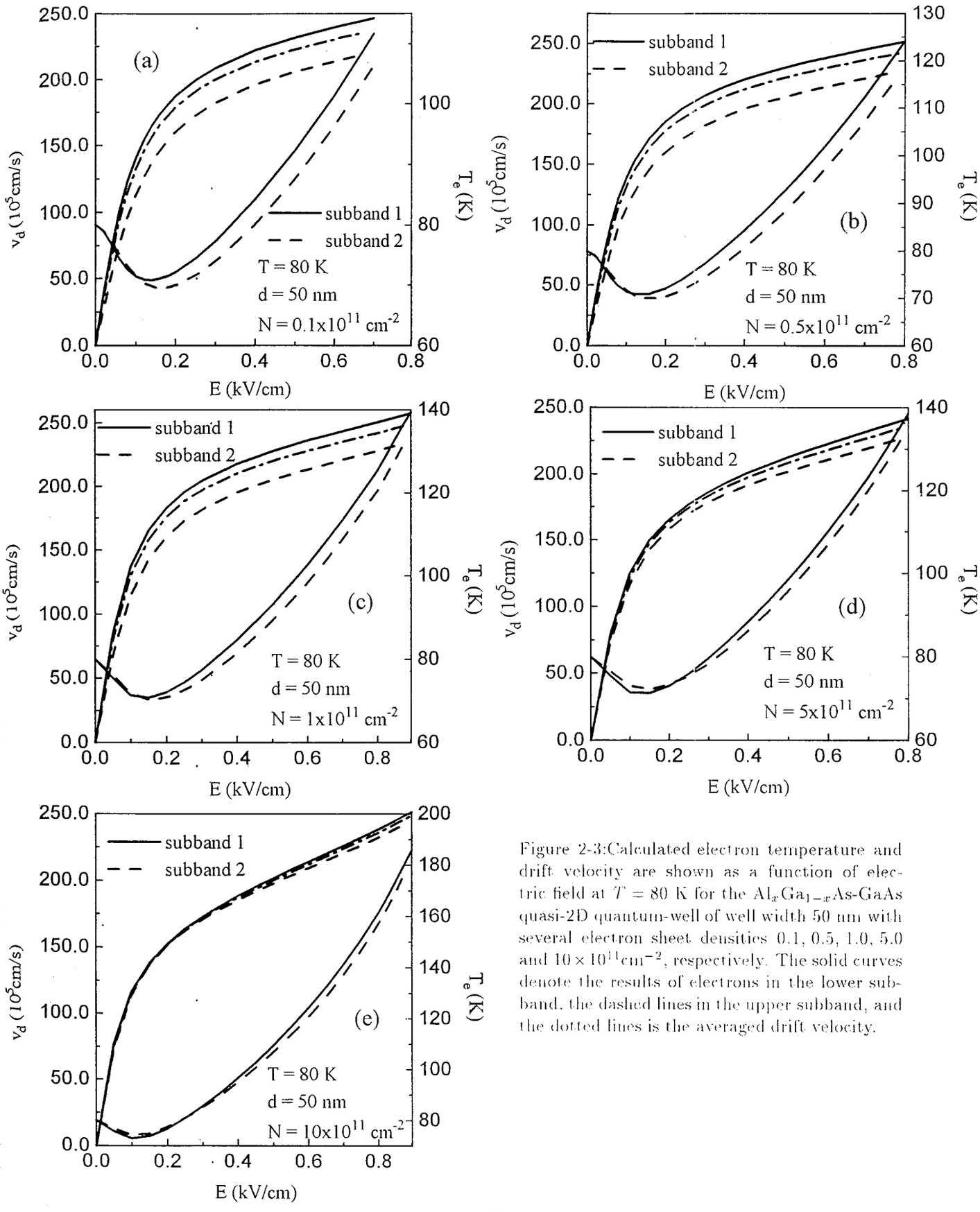

Figure 2-3:Calculated electron temperature and drift velocity are shown as a function of electric field at $T = 80$ K for the $Al_xGa_{1-x}As$-GaAs quasi-2D quantum-well of well width 50 nm with several electron sheet densities 0.1, 0.5, 1.0, 5.0 and $10 \times 10^{11} cm^{-2}$, respectively. The solid curves denote the results of electrons in the lower subband, the dashed lines in the upper subband, and the dotted lines is the averaged drift velocity.

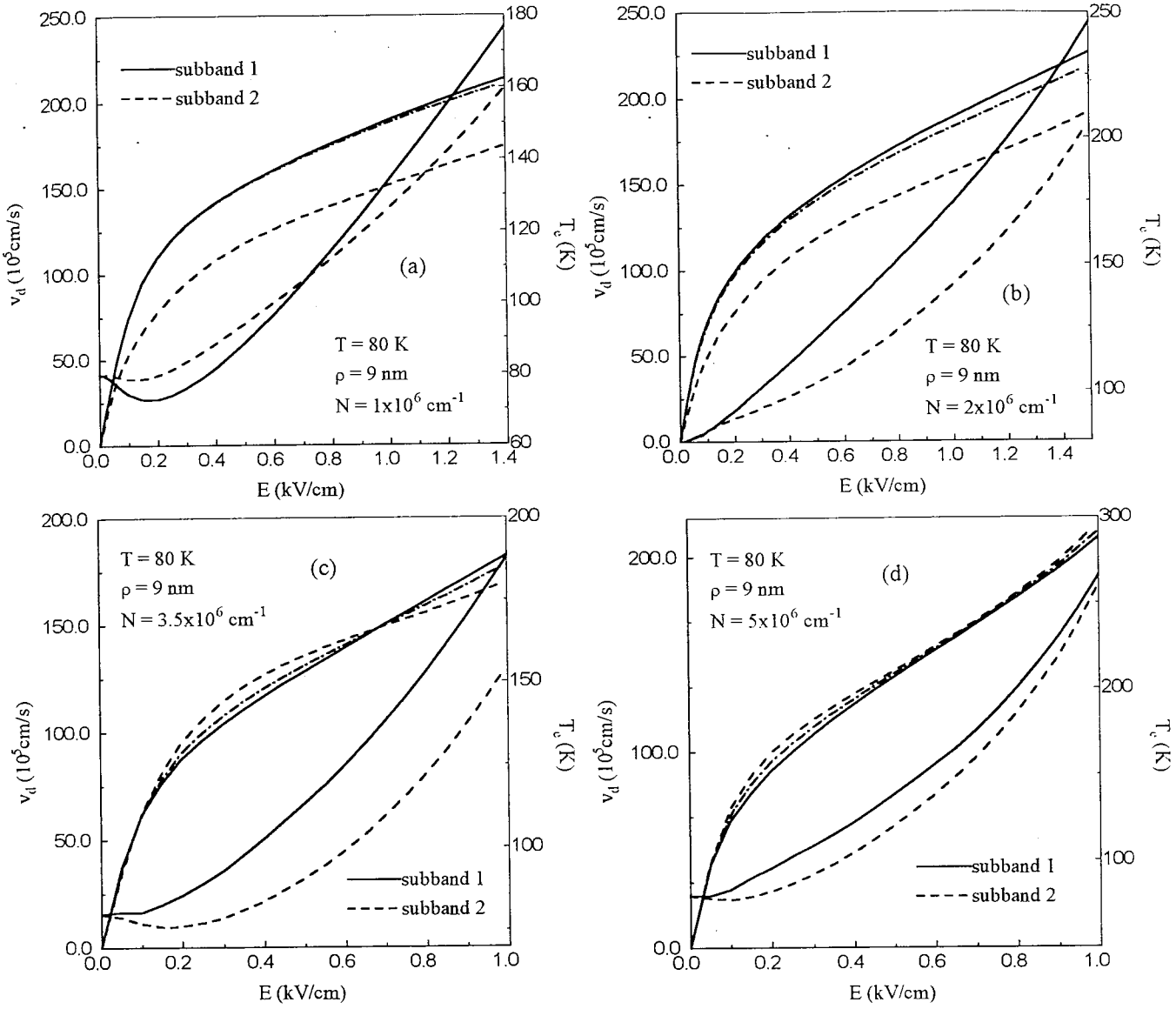

Figure 2-4: Calculated electron temperature and drift velocity are shown as a function of electric field at $T = 80$ K for the $Al_xGa_{1-x}As$-GaAs quasi-1D quantum-wire of radius 9 nm with several electron line densities 1.0, 2.0, 3.5 and $5.0 \times 10^6 cm^{-1}$, respectively. The solid curves denote the results of electrons in the lower subband, the dashed lines in the upper subband, and the dotted lines is the averaged drift velocity.

Generally, the electron temperatures and drift velocities in different subbands are not equal due to finiteness of the carrier intersubband Coulomb interaction. The difference of these quantities of different subbands depends on the gap between the ground and first excited subbands and on the electron density. In these figures, we focus our attention on the effects of the electron density. It is believed that the higher the electron density the stronger the intercarrier Coulomb interaction. It is easily seen from Fig.2-3(a) that in the case of electron density $N_s = 0.1 \times 10^{11}$ cm^{-2}, there are great disparities of both the electron temperatures and drift velocities between two subbands. When the electron density gradually become more and more high, the temperature and drift velocity of electrons within the first excited subband are more and more close to those of electrons dwelling in the ground

subband. These figures apparently show that in the case of higher electron density, $N_s = 5.0$ and 10×10^{11} cm^{-2}, these disparities are largely reduced. Similar conclusion can be drawn from the results of quantum-wire systems. In Figs.2-4 we plot electron temperatures and drift velocities of separate subbands, as well as the average drift velocity v_d defined by

$$v_d = \frac{N_0 v_0 + 2N_1 v_1}{N}$$

for quasi-1D quantum wires with radius $\rho = 9$ nm having electron line densities $N_l = 1.0$, 2.0, 3.5 and 5.0×10^6 cm^{-1}, respectively. Significant change of electron temperatures and drift velocities behavior occurs in the quasi-1D case when the electron line density increases from $N_l = 1.0 \times 10^6$ cm^{-1} to $N_l = 5.0 \times 10^6$ cm^{-1}.

All these figures demonstrate that the intersubband Coulomb interaction plays a decisive role in transport of systems having two occupied subbands. If the electron density is low, the intersubband Coulomb interactions are not strong enough to rapidly thermalize electrons among the different subbands. It is thus natural that electrons in different subbands possess different electron temperatures, drift velocities and chemical potentials when an external electric field is applied. This implies that the presumption of the OTCM is invalid for the case and the TTCM must be used to solve the transport problems for systems of low electron density. On the contrary, in the case of the high electron density, the electrons thermalization between the first and second subbands is so rapid due to the strong intersubband Coulomb scatterings that electrons dwelling within different subbands share a common electron temperature after the system comes to a stationary state under a uniform external electric field. Obviously, OTCM is a good approximation for such systems. Therefore, it is the electron density that is the decisive factor of the validity of the simplified OTCM for a given low-dimentional system.

2.5.2 Dependence on the Confinement

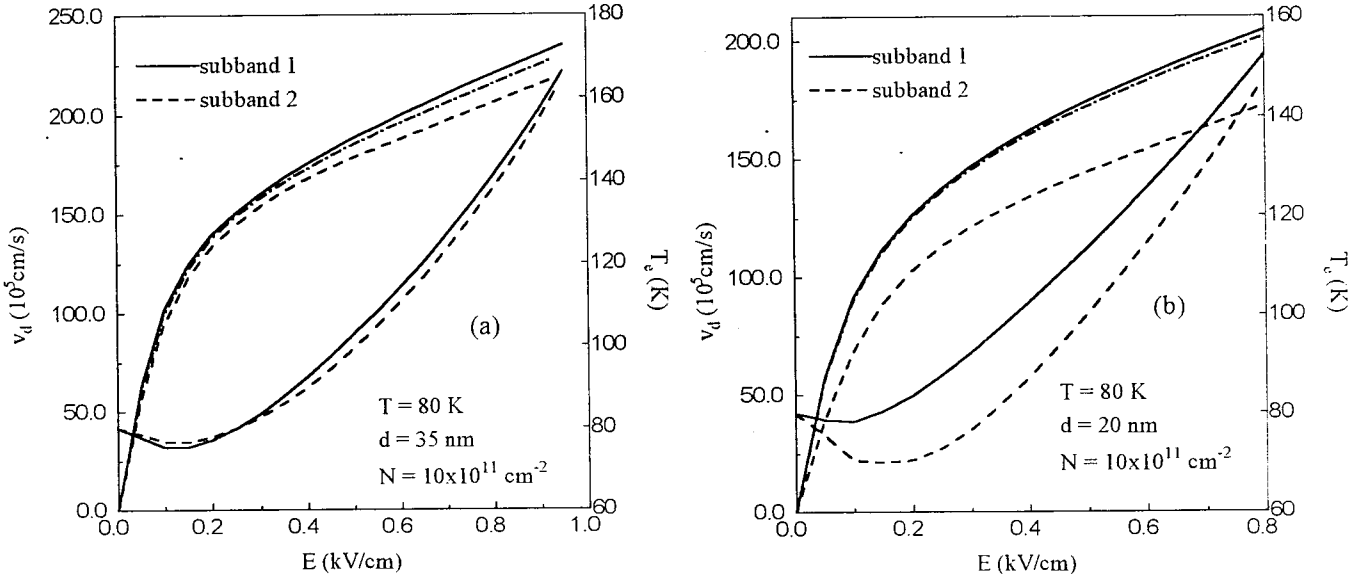

Figure 2-5: Calculated electron temperature and drift velocity are shown as a function of electric field at $T = 80$ K for the $Al_xGa_{1-x}As$-GaAs quasi-2D quantum-well of a electron sheet density 10×10^{11}cm^{-2} with two different well widths $d = 35$ and 20 nm, respectively. The solid curves denote the results of electrons in the lower subband, the dashed lines in the upper subband, and the dotted lines is the averaged drift velocity.

In this subsection, we will investigate the dimensionality dependence of the validity of OTCM for low-dimensional systems. It is well-known that the confinement of a low-dimensional system is more strong, the gap between the ground and the first excited subbands is more great. Then, more strong inter-subband scatterings are needed to make electrons dwelling within different subbands thermalize for the system with a given carrier density. In other words, for a system with a given carrier density, as the confinment become stronger, the disparity of transport properties of electrons between the two lowest subbands become more obvious. The numerical calculations, depicted in Fig.2-5 for quasi-two-dimensional quantum wells and Fig.2-6 for quasi-one-dimensional quantum wires, prove this argument.

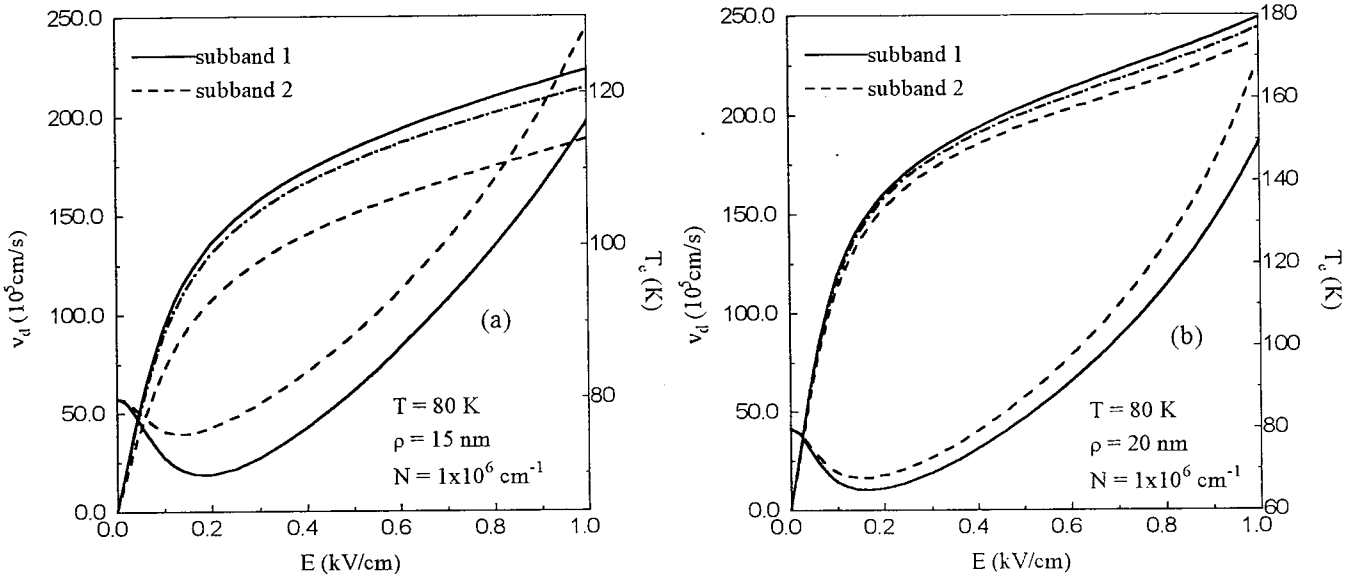

Figure 2-6: Calculated electron temperature and drift velocity are shown as a function of electric field at $T = 80$ K for the $Al_xGa_{1-x}As$-GaAs quasi-1D quantum-wire of a electron line density $1.0 \times 10^6 cm^{-1}$ with two different wire radiu $\rho = 15$ and 20 nm, respectively. The solid curves denote the results of electrons in the lower subband, the dashed lines in the upper subband, and the dotted lines is the averaged drift velocity.

In Fig.2-5, we calculate the drift velocities and electron temperatures for the two lowest subbands of the quatum wells with electron density $N_s = 10 \times 10^{11}$ cm^{-2} and two different well-width $d = 20$, 35 nm at the lattice temperature of 80 K, respectively. We can deduce, from above subsection, that for the quatum well with well-width $d = 50$ nm ($\varepsilon_{10} = \varepsilon_1 - \varepsilon_0 = 6.7$ meV) the electron density $N_s = 10 \times 10^{11}$ cm^{-2} is enough high to make electrons between the two lowest subbands nearly share a common drift velocity and electron temperature. However, when the well width become thiner, for example, $d = 35$ ($\varepsilon_{10} = 13.7$ meV) and 20 nm, diference between the two lowest subbands grow. It is clear that for the quantum well with $d = 20$ nm ($\varepsilon_{10} = 40$ meV) the OTCM is no more valid. Similar results for quatum wires can be obtained from Fig.2-6, in which the drift velocities and electron temperatures are plotted as functions of external electric fields for quatum wires with electron density $N_l = 1 \times 10^6$ cm^{-1} and $\rho = 15$ ($\varepsilon_{10} = 22.5$ meV) and 20 nm ($\varepsilon_{10} = 12.7$ meV).

2.5.3 Chemical Potential and Subband Occupancy under External Electric Fields

In above two subsections, we pay our main attention to the two coefficients, the center-of-mass averaged drift velocity and the electron temperature, which are the fundamental physical quantities in

the nonlinear transport field of semiconductor. In low-dimensional systems, due to size quantization, the quantized energy levels, subbands, are formed and one can focus interest upon the electron occupancy of each subband under external electric fields. Here we use the Lei-Ting balance equations to investigate the electron population, i.e., the chemical potentials of each subband which are used as auxiliary coefficients in the Lei-Ting balance-equation theory, in the two lowest subbands in quasi-two-dimensional quantum well systems.

Figs.2-7 illustrate our numerical results for $d = 50$ nm quantum wells with a series of electron densities. The electron populations in the two subbands of OTCM are also plotted in these figures in comparison with those of TTCM. It is surprising that the chemical potentials of the two subbands keep still regular dissimilarity, instead of becoming identical just as the drift velocities and electron temperatures do in Figs.2-3, as the electron density increases gratually from low to high. In the case of electron densities $N_s = 0.1$, 0.5 and 1×10^{11} cm^{-2}, the uper-subband chemical potential is higher than the lower-subband one at the whole range of electric fields. Correspondingly, the lower-subband electrons are continuously transfered to the uper-subband by the electric field. We can interpret this behavior as following. The corresponding Fermi energies above the bottom of the lowest subband at absolute zero temperature are 0.4, 4.3 and 5.2 meV, respectively, all of which are smaller than the spacing between the lowest and uper subbands, 6.7 meV for the $d = 50$ nm quantum well. Most of electrons populate in the lowest subband and only few electrons dewell in the uper subband at thermal equilibrium state. When the external electric field is applied, the lower- and uper-subbands begin to transfer electrons each other. However, the uper-subband can not supply enough electrons to offset those it gain from the lower-subband although the electron temperatures become lower than the lattice temperature at low electric field. Therefore, electrons are always pumped from the lower-subband to the uper-subband as the electric field increases. It is obvious that this behavior is inconsistent with that of OTCM. In the case of OTCM, the electron population, i.e., the chemical potential, only is the function of electron temperature T_e, $N_i = \sum_{\mathbf{k}\sigma} f\left(\left(\varepsilon_{i\mathbf{k}} - \mu\right)/T_e\right)$, due to the constant total electron sheet density N_s. Then the electron occupancy in the lower-subband always rises due to cooling effect at low electric fields in the case of three considered electron densities.

The situation is different in Figs.2-7 (d) and (e). For electron densities $N_s = 5.0$ and 10×10^{11} cm^{-2}, the Fermi levels at absolute zero temperature are 12.3 and 21.2 meV, respectively, both of which are greater than the spacing between the lower- and uper-subbands. Therefore, there are still a lot of electrons populated in the uper-subband even at very low temperatures and then the electrons in the uper-subband are more enough to sustain transfering to the lower-subband due to the cooling effect at low electric fields, such is in quanlitative agreement with the OTCM. Yet, the chemical potential of the uper-subband does not become quantitatively closer to that of the lower-subband as the electron density increases. In the case of electron density $N_s = 5.0 \times 10^{11}$ cm^{-2}, the chemical potential of the lower-subband rises above that of the uper-subband befor the electric field crosses around 0.3 kV/cm. While the chemical potential of the lower-subband keepes always lower than that of the uper-subband at the whole range of electric fields for electron density $N_s = 10 \times 10^{11}$ cm^{-2}.

This series of figures indicate that the OTCM can not well describe the behavior of electron occupancy in subbands for quantum wells with well width $d = 50$ nm in the case of higher electron density than 1.0×10^{11} cm^{-2}, although the meticulous model (TTCM) showes that different subbands tend to a common drift velocity and electron temperature. It seems that the approach extended by Guillemot[27] based on the Lei-Ting balance-equation theory, assuming that different subbands share a unique drift velocity and electron temperature but posses different chemical potentials, is more appropriate for investigation of transport in quantum wells in the multisubband populated case than the OTCM.

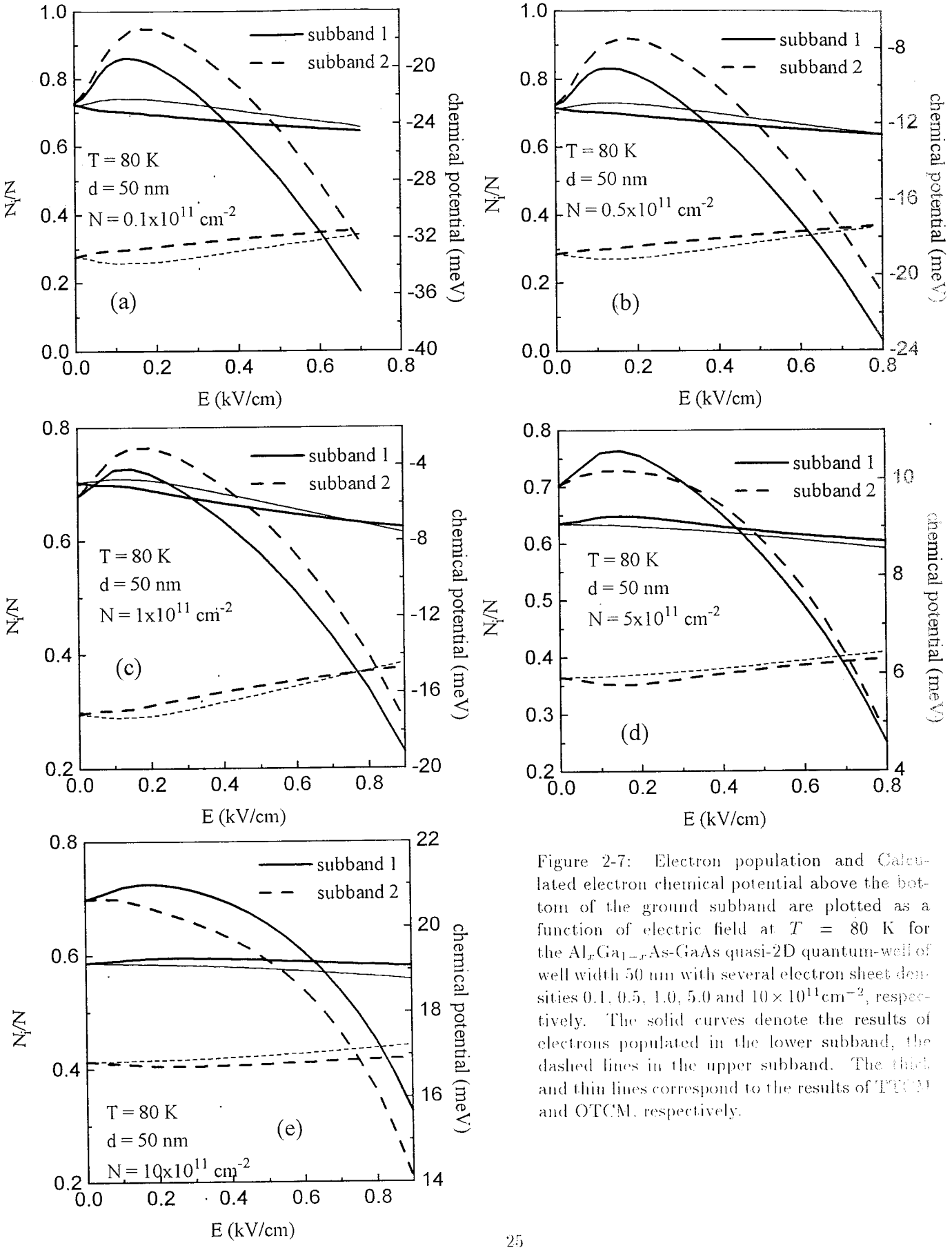

Figure 2-7: Electron population and Calculated electron chemical potential above the bottom of the ground subband are plotted as a function of electric field at $T = 80$ K for the $Al_xGa_{1-x}As$-GaAs quasi-2D quantum-well of well width 50 nm with several electron sheet densities 0.1, 0.5, 1.0, 5.0 and $10 \times 10^{11} cm^{-2}$, respectively. The solid curves denote the results of electrons populated in the lower subband, the dashed lines in the upper subband. The thick and thin lines correspond to the results of TTCM and OTCM, respectively.

2.5.4 Intersubband Coulomb Scattering in Linear Mobility in Quantum Wells

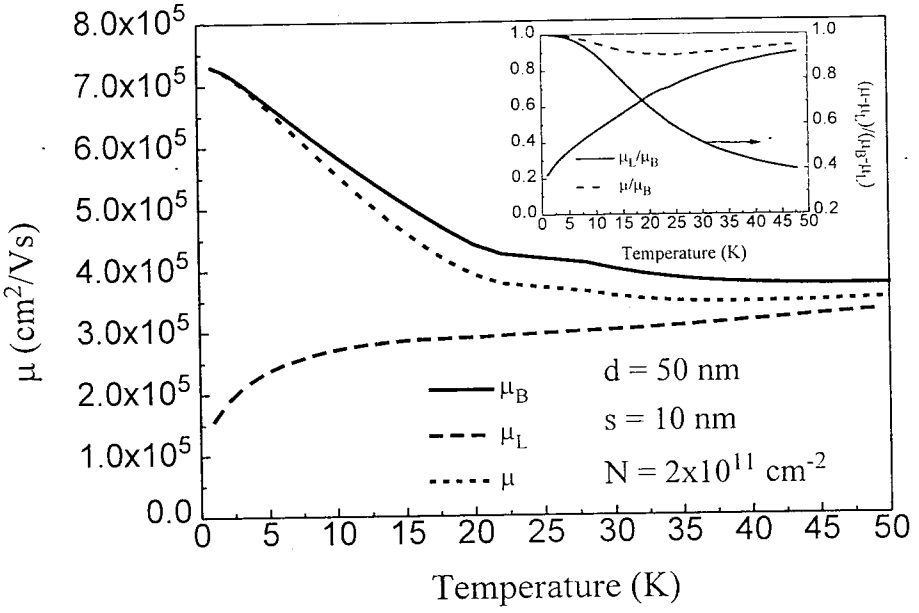

Figure 2-8: Mobilities μ, μ_B and μ_L are plotted as a function of lattice temperature in a $Al_xGa_{1-x}As$-GaAs quasi-2D quantum-well of well width 50 nm with electron sheet density $2 \times 10^{11}cm^{-2}$, and distance $s = 10$ nm of the remote impurity layer from the center of the well. The solid curve denotes μ_B, the dashed line μ, and dotted line μ_L. Inset: μ_L/μ_B (solid line), μ/μ_B (dashed line) and $(\mu - \mu_L)/(\mu_B - \mu_L)$ (solid line) as a function of lattice temperature.

In this subsection, we invesitgate the effect of intersubband electron-electron Coulomb interaction on the linear transport, i.e., the mobility. The Eq.(2.37) evidently tell us that the intersubband Coulomb interaction has a direct contribution to the total mobility of quantum wells in the case of two subbands occupied.

Here we are interested in two limit cases: weak and strong intersubband Coulomb interaction[42]. For the sake of simplicity, the intersubband electron-phonon scatterings are neglected in the following formulae. However, in practical evaluation, these scattering mechanism should be included. First, for the weak intersubband Coulomb interaction case $F_{12} \to 0$, in which the Boltzmann equation is valid, the mobility μ is simplified as

$$\mu_B = \frac{-e}{N}\left(\frac{N_1^2}{F_1'} + \frac{N_2^2}{F_2'}\right). \tag{2.74}$$

which is identical to the result of two-band model of Boltzmann equation[33] and hence is called Boltzmann mobility μ_B. On the contrary, for the strong intersubband Coulomb interaction case $F_{12} \to \infty$, we can find that only if $v_1 = v_2$ the group of equations (2.34) and (2.35) are solvable and this is consistent with physical concept that the enough strong intersubband electron-electron interaction can induce intersubband rapid thermalization. In this situation electrons dewelling in different subbands are handled as a whole and OTCM is valid. And the mobility μ tends to the Lei-Ting mobility μ_L of OTCM:

$$\mu_L = -Ne\frac{1}{F_1' + F_2'}. \tag{2.75}$$

The two definitions Eqs.(2.74) and (2.75) are apparently different and represent two extreme cases of the intersubband electron-electron interaction strength in quantum wells. Unfortunately, the strength of the intersubband Coulomb interaction is neither zero nor infinity and the real mobility must be calculated from Eq.(2.37). Nevertheless, the disparity among three mobilities can demonstrate that how the intersubband Coulomb scattering can affect transport properties and give a hint for further simplification.

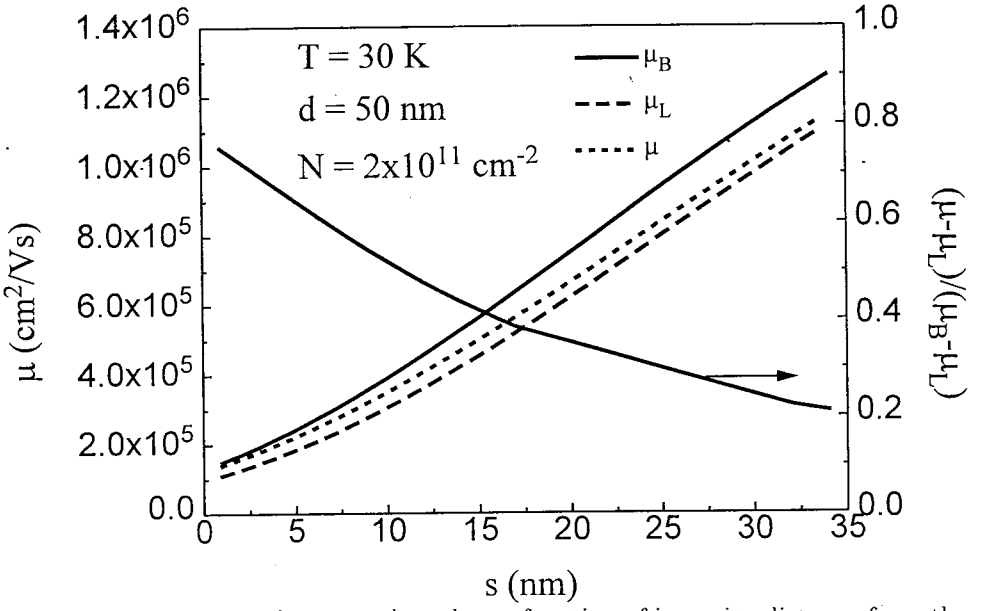

Figure 2-9: Mobilities μ, μ_B and μ_L are plotted as a function of impurity distance from the center of the well of well width 50 nm with electron sheet density $2 \times 10^{11}\text{cm}^{-2}$ at the temperature of 30 K. The solid curve denotes μ_B, the dashed line μ, and dotted line μ_L. Inset: $(\mu - \mu_L)/(\mu_B - \mu_L)$ (solid line) as a function of impurity distance from center of well.

In Fig.2-8, we evaluate the real mobility μ, Boltzmann mobility μ_B and Lei-Ting mobility μ_L as a funciton of the lattice temperature in a quantum well, width $d = 50$ nm, electron sheet density $N = 2 \times 10^{11}$ cm^{-2}, for distance $s = 10$ nm of the remote impurity layer from the center of the well. At the whole range of the lattice temperature, the overall bahaviour of μ is similar with μ_B. μ_L has a completely different temperature-dependence at extremely low temperature and with the increasing of temperatures it tends close to the others. The inset shows the behaviour more clearly. This means that at the extremely low temperature, the intersubband electron-electron scattering is significantly weaker than the impurity scattering and with the increasing of temperature the impurity scattering becomes lower, while the electron scattering higher. So the temperature is another factor which can affect the intersubband Coulomb interaction. We can deduce that for a very clean sample, the impurity scattering is always weak in comparison with the electron scattering, then the μ_L has a similar behaviour with the μ_B at the whole range of tempertures. Fig.2-9 illustrates the three mobilities as a function of remote impurity distance s from the center of the quantum well. The μ_B is generally larger than the μ_L because electron-electron scattering tends to scatter "runaway" electrons with large velocities (where the impurity scattering rate is small) back into lower velocity states. As s becomes larger, the electron-electron scattering dominates over all other scattering mechanisms and

$\mu \rightarrow \mu_L$. Conversely, for small s, the impurity scattering is relatively large compared to the electron-electron scattering, and μ is closer to the μ_B than μ_L. The crossover from μ_B to μ_L is also shown in this figure.

2.6 Conclusion

In this chapter, a systematically investigation about the effects of the inter-subband Coulomb interaction on the linear and nonlinear transport in quasi-two-dimensional quantum well and quasi-one-dimensional quantum wire systems with different electron densities and confinments has been performed by using the two-types-of-carriers model of Lei-Ting balance-equations theory. We have found that, when the electron density rises, the enhanced inter-subband Coulomb scattering can make the electrons among different subbands thermalize and achieve a common drift velocity and electron temperature. This gives a judgement which decides whether or not the OTCM is validity for invesitgation of transport in low-dimensional multisubband systems. In addition, the effect of the confinement on the inter-subband interactions in low-dimensional systems has also been discussed. By analyzing the linear mobility in quantum wells, we can demonstrate the effect of temperatures on the inter-subband interactions and a well-defined crossover from μ_B to μ_L.

Moreover, taking quasi-two-dimensional quantum wells as example, we have researched into the electron occupancies and chemical potentials in each subbands under external electric fields. We find that the chemical potentials between the two lowest subbands always keep distinguishable from low to high electron densities and this distinguishable can not be removed by the enchanced inter-subband Coulomb interaction. However, it should be noted that the TTCM extended by us in this paper include only the dominant inter-subband Coulomb interaction term, in which the two electrons dewelling in different initial subbands scatter but keep staying within their respective subbands after scattering. This inelastic scattering between subbands allows energy to be transferred from hot subbands to cold subbands so that a uniform energy is quickly reached between different subbands. Those results obtained in Secs.2.5.1 and 2.5.2 are qualitatively consistent with this conceptual viewpoint. Due to not involve exchange of particles between different subbands, this inter-subband Coulomb interaction term can not directly contribute to the rate of change of particle number. The exchange of particles between different subbands is caused only by inter-subband electron-phonon interactions. It is well-known that, the electron-phonon interactions are no related to the electron density and weaker than the electron-electron interactions. Therefore, it is easy understood that the calculated chemical potentials in the two lowest subbands always keep disparity even though the electron density rises (Figs 2-7). On the other hand, in order to more careful inspection of electron occupancy in subbands, we must investigate those profound inter-subband Coulomb interaction terms involving exchange of particles between different subbands. The further topic how to include these profound inter-subband Coulomb interactions in Lei-Ting balance-equations theory is our task in the future.

Chapter 3

Electron Noise Temperature in Heterjunction

3.1 Background

Thermal noise is an important problem in Semiconductor Physics[50, 51]. Especially, when the size of the device is small and the electric field across the terminals becomes strong, thermal noise is a crucial consideration which can determine the reliability of the device. Unfortunately, even though the noise problem in a low electric field has been intensively studied, its knowledge in high-field region is still very poor. In recent years, a quasianalytical method on the thermal-noise problem in steady-state transport in the presence of a dc electric field has been derived through the Langevin-type equation for the fluctuation center-of-mass velocity operator by Hu[53] and Lei[52], separatedly. Both of their works are based on the Lei-Ting balance-equation approach.[37] Their theory bears no relation to the strength of the applied dc electric field. Hence, they can use it to investigate the thermal-noise problem under high electric fields. From their equations, the same result as Nyquist relation is re-obtained at low fields, but at high-field region a modified expression for the fluctuation-dissipation theorem must be produced to replace the standard one. Furthermore, their method can be extended to discuss the effect of nonequilibrium phonon occupation (hot-phonon effect) on the thermal noise.

In recent years, thanks to the technological advance, it becomes possible the real application of the low-dimensional devices. As mentioned in the previous paragraph, thermal noise is a great important limitation for these small size devices. One of authors[25] has systematically discussed the thermal-noise temperature in steady-state nonlinear transport in GaAs-AlGaAs single-layer and multilayer heterosystems with and without hot-phonon effect. However, they considered the contribution of electrons occupying only the lowest subband in their evaluation. Unfortunately, the occupation of more than the lowest subband in low-dimensional systems has a great influence on transport properties of electrons, of course on the thermal-noise problem. Thus it is necessary to extend the method of investigating the thermal-noise problem of low-dimensional systems to the case of multi-subband occupations of carriers.

Recently, many authors studied electron transport properties of low-dimensional systems considering multi-subband occupied cases. In most balance-equation investigations on these problems, electrons in different subbands are assumed to share a common electron temperature, chemical potential and average drift velocity based on the presumption of sufficiently rapid thermalization of electrons among different subbands. In our recent paper[48] and Chapter 2 of the thesis, a systematic theoretical investigation on the validity of this presumption for low-dimensional multi-subband systems has been carried out by means of the balance-equation approach of the two-types-of-carriers model (TTCM). We can draw conclusion from the paper that the validity of the presumption is crucially dependant

upon the electron density and the confinement of low-dimensional systems and if the electron density is high enough, how high the density is needed is related to the confinement of low-dimensional systems, the one-type-of-carriers model (OTCM) is a good approximation for low-dimensional multi-subband systems. In this chapter, we will first use the same approach to detailedly study electron transport in heterojunctions with two electron densities $N_s = 1.9$ and 5.7×10^{11} cm^{-2} at the lattice temperature of 80 K and to show that in the case of densities OTCM is applicable to describing electron transport in Heterojunctions. Therefore, we can apply the much more simple model, i.e., OTCM, to study thermal noise of quasi–two-dimensional heterojunction systems having multi-subband occupations. A brief discussion about the thermal noise problem in quasi-two-dimensional case is provided. In the following, it is extended to apply to the case of muli-subband occupied, detailed numerical investigation is carried out for Heterojunction and the current results are compared with those of only considering one-subband occupied case.

3.2 Electron Transport in Heterojunctions for the Two-Subband Occupied Case

First, we are intend to use the approach given in above chapter to investigate electron transport in heterojunctions. Consider a single $Al_xGa_{1-x}As$-$GaAs$ heterostructure system and use the Fang-Howard-Stern variation wave function:[54]

$$\zeta_0(z) = \left(\frac{b_0^3}{2}\right) z \exp\left(-\frac{b_0 z}{2}\right) \tag{3.1}$$

and

$$\zeta_1(z) = \frac{3}{2}\left(\frac{b_1^5}{b_0^2 - b_0 b_1 + b_1^2}\right)^{1/2} z\left[1 - \left(\frac{b_0 + b_1}{6}\right) z\right] \exp\left(-\frac{b_1 z}{2}\right) \tag{3.2}$$

as the envelope wave functions for the $n = 0$ and $n = 1$ subbands, respectively. The variational parameters b_0 and b_1 and subband energies ε_0, ε_1 due to the quantized motion in the z direction are determined by a variational calculation[55].The electron subband energy can be expressed as:

$$\varepsilon_{n\mathbf{k}} = \varepsilon_n + \frac{\hbar^2}{2m^*} k^2 \tag{3.3}$$

Fig.3-1, which depicts the square of form factors of intra- and inter-subband Coulomb interactions in heterojunction as a function of q, showes that the square of the form factors of the third class are nearly two orders of magnitude smaller than those of other two classes. Therefore, the same balance equations for the force, energy and particle number are obtained as those derived in quantum wells given in above chapter, except for the form factors involved due to the different wave functions in heterojunctions.

In Fig.3-2 and 3-3, we plot the calculated normalized electron temperatures and drift velocities of two subbands as functions of external electric fields for a $Al_xGa_{1-x}As$-$GaAs$ heterostructure system with carrier sheet densities $N = 1.9$ and 5.7×10^{11} cm^{-2}, respectively. All solid curves are the values of electrons within the ground subband 0, all dash curves are those of electron dwelling in the first excited subband 1 and dash-dotted lines correspond to the average drift velocities v_d:

$$v_d = \frac{N_0 v_0 + N_1 v_1}{N}.$$

In these calculations, we assume the remote impurity densities are a half of the electron densities. For comparison, we have also performed numerical calculations for the same systems using the OTCM balance-equations, i.e. assuming a common center-of mass velocity, a single electron temperature and

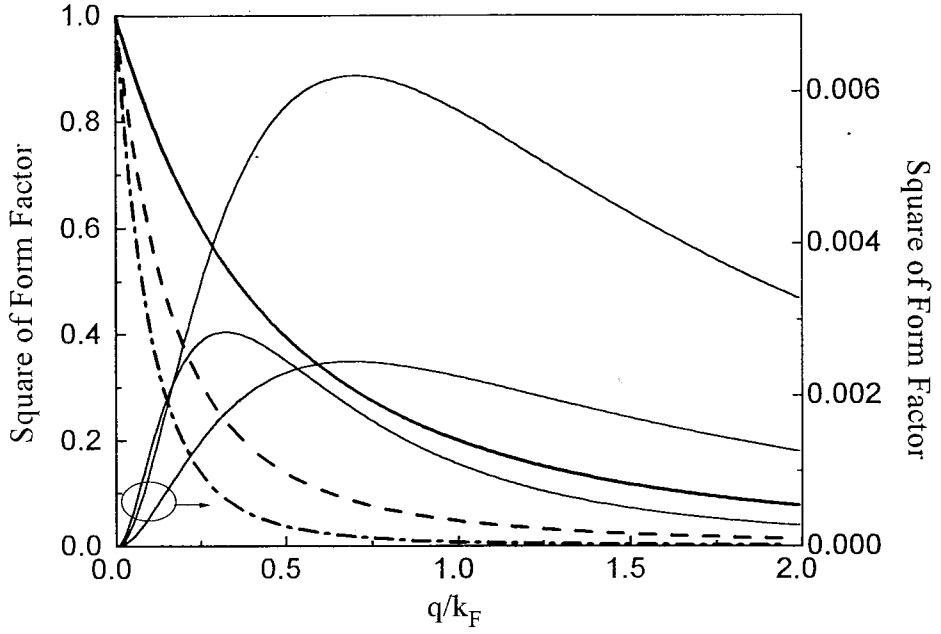

Figure 3-1: Form factors of e-e Coulomb interactions for $Al_xGa_{1-x}As$-$GaAs$ heterostructure with electron sheet density $N = 5.7 \times 10^{11}\ cm^{-2}$ versus the normalized wave vector q/k_F (k_F is the absolute zero temperature Fermi wave vector) are plotted. The thick solid line stands for $|H_{00,00}(q)|^2$, the dashed line for $|H_{11,11}(q)|^2$ and the dashed-dotted line for $|H_{00,11}(q)|^2$. All thin solid curves denote form factors of the third class of the e-e Coulomb interactions.

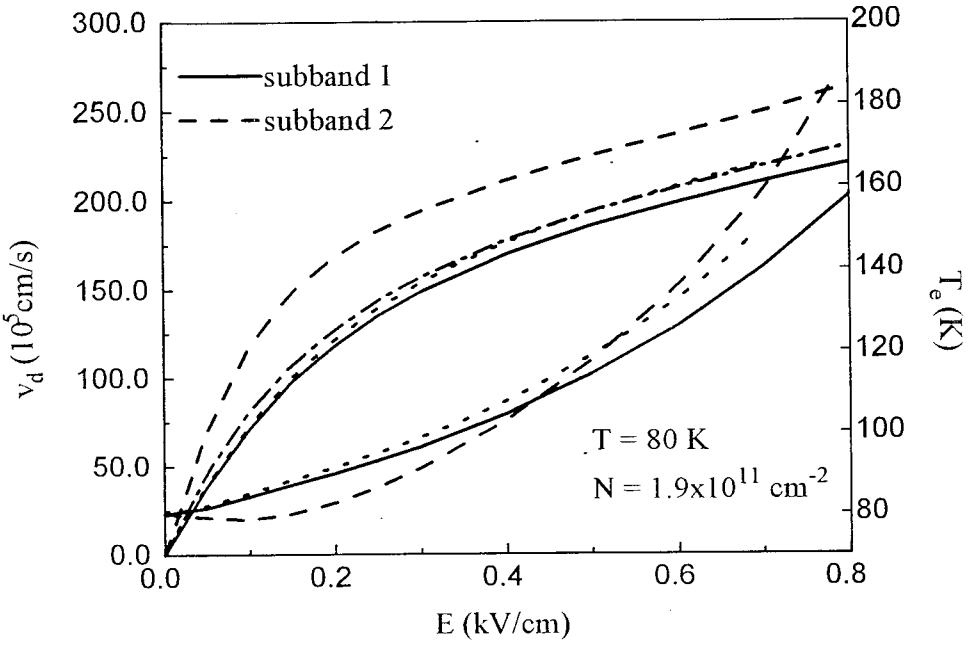

Figure 3-2: Calculated drift velocity and electron temperature are shown as a function of electric field at $T = 80$ K, including the contributions of the intersubband e-e Coulomb interactions. The electron sheet densities are 1.9×10^{11} cm^{-2} (thick lines). The solid lines denote the results of electrons in the lowest subband, the dashed lines in the upper subband. The dashed-dotted line stands for the averaged drift velocity. The dotted curves represent those results of OTCM.

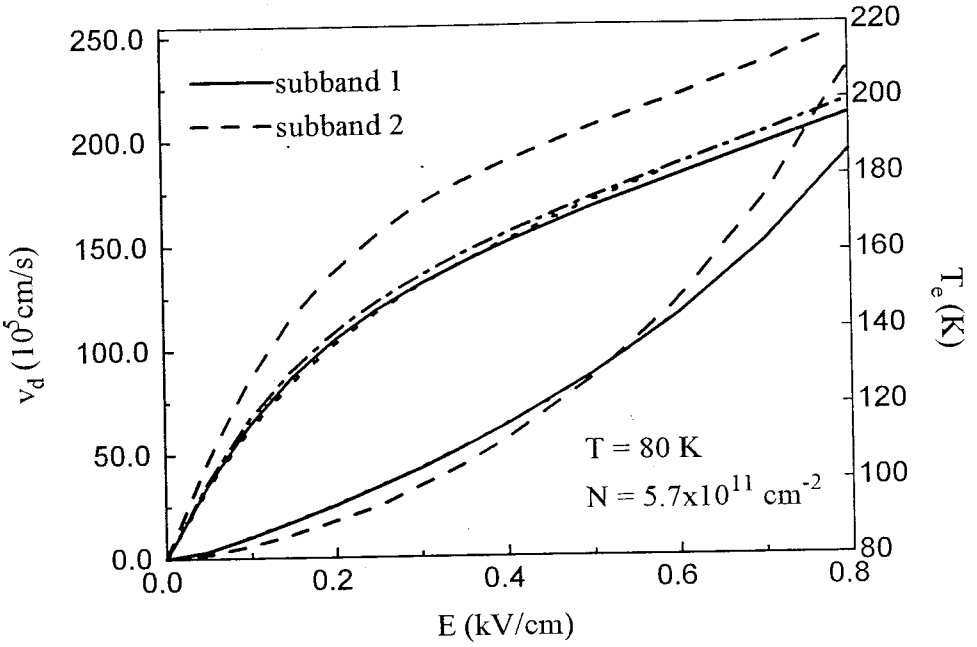

Figure 3-3: The same as Fig.3-2 except for the electron sheet density of 5.7×10^{11} cm^{-2}.

a unique Fermi level for all the electrons in different subbands, which are shown by dots in these figures. Generally speaking, the electron temperatures and drift velocities of electrons in different subbands obtained by using TTCM method are not equal at the whole electric field region for various electron sheet densities and they are also different from those obtained by using OTCM method. Figs.3-2 and 3-3 clearly indicate that, for the calculated electron densities $N = 1.9$ and 5.7×10^{11} cm^{-2}, there are great difference between the drift velocities of the ground subband and the upper subband even at the weaker electric fields. However, frome the two figures, we can also evidently see that the averaged drift velocities for the two heterojunction systems are nearly equal to the drift velocities of OTCM at the whole electric fields. Moreover, the difference for the electron temperatures between the two subbands is only a little when the electric field is not very strong. Especially in the case of the electron density 5.7×10^{11} cm^{-2}, the behavior of electrons of OTCM is approximately identical to electrons within the ground subband of TTCM. From this point in view, we can conclude that OTCM can well describe the behavior of electron transport in heterjunction systems with carrier sheet densities of 1.9 and 5.7×10^{11} cm^{-2}. Therefore, for the sake of simplicity, OTCM is a enough good model to investigate more profound transport properties in heterjunction systems, such as thermal noise temperature, which is the main topic concerned in the following sections.

3.3 Balance Equation Theory for Thermal Noise Temperature

Consider an electron-phonon system, composed of N interacting electrons in the presence of a uniform electric field. As the procedure in section 2 of the first chapter, we can separate the electronic degrees of freedom into a center-of-mass part (H_c) and a relative electron part (H_r). With the help of Heisenberg equation, the rate of change of the center-of-mass momentum P is given by

$$\dot{\mathbf{P}} = -\frac{i}{\hbar}[\mathbf{P}, H_c + H_r + H_{ph} + H_I] = Ne\mathbf{E} + \hat{\mathbf{F}}, \tag{3.4}$$

where $\hat{\mathbf{F}} = \hat{\mathbf{F}}_i + \hat{\mathbf{F}}_p$ is the frictional-force operator with $\hat{\mathbf{F}}_i$ and $\hat{\mathbf{F}}_p$ correspoding to impurity and phonon contributions, respectively. Similarly, the Liouville equation for the statistical density matrix ρ of the relative electron-phonon system takes the form

$$i\frac{\partial \rho}{\partial t} = [H_c + H_e + H_I, \rho], \tag{3.5}$$

and the initial condition for the density matrix ρ is chosen as

$$\rho|_{t=-\infty} = \rho_0 = \frac{1}{Z_e} e^{-H_e/T_e} \frac{1}{Z_{ph}} e^{-H_{ph}/T}. \tag{3.6}$$

However, the center-of-mass, being a single particle of enormous mass performing Brownian motin, can be described classically by its instantaneous position and velocity. In order to investigate the thermal noise and diffusion problem, the drift velocity of center-of-mass can be written as the sum of a constant drift velocity $\mathbf{v}_d$ and a small fluctuation part $\delta\hat{\mathbf{V}}(t)$ in steady transport state

$$\mathbf{V}(t) = \mathbf{v}_d + \delta\hat{\mathbf{V}}(t), \tag{3.7}$$

instead of only the constant drift velocity as done in the above chapter. Obviously, the ensemble average of $\delta\hat{\mathbf{V}}(t)$ is

$$\left\langle \delta\hat{\mathbf{V}}(t) \right\rangle = 0. \tag{3.8}$$

Considering the rate of change of the center-of-mass $\dot{\mathbf{P}}(t) = Nmd\mathbf{V}(t)/dt = Nmd\delta\mathbf{V}(t)/dt$, we can rewritten the Eq.(3.4) in the Hersenberg representation:

$$Nm\frac{d}{dt}\delta\mathbf{V}(t) = Ne\mathbf{E} + \hat{\mathbf{f}} + \hat{\mathbf{F}}(t) + Nm\int_{-\infty}^{t} \underline{\hat{\mathcal{K}}}(t-s)\cdot\delta\hat{\mathbf{V}}(s)ds, \tag{3.9}$$

in which $\hat{\mathbf{f}}$ is a time-dependent force operator and $\underline{\hat{K}}(t)$ is a time-dependent tensor operator. To the lowest order of (electron-impurity and electron-phonon) interactions, the operator $\hat{\mathbf{f}}$ and $\underline{\hat{\mathcal{K}}}(t)$ in the Eq.(3.9) can be replaced by their ensemble average $\mathbf{f}$ and $\mathcal{K}(t)$. $\hat{\mathbf{F}}(t)$ is the fluctuation force along the same direction as the random velocity $\delta\mathbf{V}(t)$.

Taking the ensemble average of Eq.(3.9), the force balance equation

$$Ne\mathbf{E} + \mathbf{f} = 0, \tag{3.10}$$

can be derived, which determines the dc bias point: drift velocity $\mathbf{v}_d$ and electron temperature T_e , together with the energy balance equation, in the presence of a dc field $\mathbf{E}$. With this in view, Eq.(3.9) becomes a Langevin-type equation connecting the random velocity $\delta\mathbf{V}(t)$ and the fluctuation force $\hat{\mathbf{F}}(t)$, which are resolved into two components of parallel to (longitudinal component) and perpendicular to (transverse component) the external dc electric field $\mathbf{E}$,

$$\frac{d}{dt}\delta\hat{V}_{\parallel(\perp)}(t) = \frac{1}{Nm}\hat{F}_{\parallel(\perp)}(t) + \int_{-\infty}^{t} \mathcal{K}_{\parallel(\perp)}(t-s)\delta V_{\parallel(\perp)}(s)ds. \tag{3.11}$$

We can solve this equation by Fourier transformation, yielding

$$\delta\hat{V}(\omega) = \frac{1}{Nne}\sigma_n(\omega)\hat{F}(\omega). \tag{3.12}$$

where n is the carrier number density and $\delta V(\omega)$ and $F(\omega)$ are the Fourier transforms of the random velocity $\delta\hat{V}(t)$ and the fluctuation force $\hat{F}(t)$, and $\sigma_n(\omega)$ is a dynamic conductivity defined by

$$\sigma_n(\omega) = i\frac{ne^2}{m}\frac{1}{\omega + M(\omega)}. \tag{3.13}$$

Here m is the effective mass of electron and $M(\omega)$ is the memory function consisting of an impurity and a phonon contributions.

From the generalized Einstein relation between the generalized diffusion coefficient $D_n(\omega)$ ($D_n(\omega) = \frac{1}{2n^2e^4}|\sigma_n(\omega)|^2 S(\omega)$) and the thermal noise temperature $T_n(\omega)$

$$D_n(\omega) = \frac{T_n(\omega)}{ne^2}\mathrm{Re}\left[\sigma_n(\omega)\right], \tag{3.14}$$

the noise temperature which means that the maximum available noise power in the frequency range $\omega \to \omega + d\omega$ of a passive two-terminal network made of the material with noise temperature $T_n(\omega)$ is $T_n(\omega)d\omega$ [25] can be simply defined as

$$T_n(\omega) = \frac{S(\omega)}{2mM_2(\omega)}, \tag{3.15}$$

where $S(\omega)$ is the Fourier transform of the symmetrized fluctuation-force correlation function, which is also composed of an impurity and a phonon contributions.

3.4 Electron Noise Temperature in Heterojunction for the Two-subband Occupied Case

Consider a single GaAs-AlGaAs heterojunction system and suppose electron transport parallel to the heterojunction plane (x-y plane). According to the balance-equation approach, a force and energy balance equations for the steady state in the presence of an electric field $\mathbf{E}$ along the x-direction are obtained:

$$Ne\mathbf{E} + \mathbf{F}(\mathbf{v}) = 0, \tag{3.16}$$

$$\mathbf{v}\cdot\mathbf{F}(\mathbf{v}) + W(\mathbf{v}) = 0, \tag{3.17}$$

where $\mathbf{v}$ is the center-of-mass velocity, or the average drift velocity of the electrons, and e and N are, respectively, the charge and the sheet density of the electrons. In these equations, $\mathbf{F}(\mathbf{v})$ is the frictional force experienced by the center-of-mass due to electron-impurity and electron-phonon interactions and $W(\mathbf{v})$ the energy transfer rate from the electron system to the phonon system. The detailed expressions for $\mathbf{F}$ and W are standard formulation for quasi-two-dimensional systems within the framework of the balance-equation approach, considering multi-subband structures, and will not be repeated here. The electron-electron Coulomb interaction is fully described in these expressions through the function $\Pi_2(nn', q, \omega)$, the imaginary part of the density-density correlation function for relative electrons $\Pi(nn', q, \omega)$, in which n and n' are subband indices and $\mathbf{q}$ is the plane wave vector $\mathbf{q} = (q_x, q_y)$. Under the random-phase approximation it can be expressed as

$$\Pi(nn', q, \omega) = \Pi^0(nn', q, \omega)\left[1 + \tilde{V}_{nn',nn'}(q, \omega)\Pi^0(nn', q, \omega)\right] \tag{3.18}$$

with the renormalized Coulomb potentials $\tilde{V}_{nn',mm'}(q, \omega)$, which satisfy the following equations:

$$\tilde{V}_{nn',mm'}(q, \omega) = V_{nn',mm'}(q) + \sum_{ll'} V_{nn',ll'}(q)\Pi^0(ll', q, \omega)\tilde{V}_{ll',mm'}(q, \omega), \tag{3.19}$$

where $\Pi^0(nn', q, \omega)$ is the density-density correlation function for electrons in the n and n' subbands in the absence of Coulomb interaction between them and $V_{nn',mm'}(q)$ the matrix elements of the bare Coulomb coupling[37, 38].

According to the treatment of the above section, the noise temperature $T_n(\omega)$ is

$$T_n(\omega) = \frac{S(\omega)}{2mM_2(\omega)} \tag{3.20}$$

for quasi-two-dimensional multi-subband systems. In the equation, $S(\omega)$ and $M_2(\omega)$ are the Fourier transform of the symmetrized fluctuation-force correlation function and the imaginary part of the memory function, respectively. Both of the two functions are composed of an impurity contribution and a phonon contribution denoted by superscript i and ph respectively:

$$\begin{aligned} S(\omega) &= S^i(\omega) + S^{ph}(\omega), \\ M_2(\omega) &= M_2^i(\omega) + M_2^{ph}(\omega). \end{aligned} \tag{3.21}$$

which may be determined, without hot-phonon effect for simplicity, as

$$\begin{aligned} S^i(\omega) = -\frac{1}{NS}\sum_{\mathbf{q}nn'} \frac{q_\alpha^2}{q^2} |U_{nn'}(q)|^2 \left[\Pi_2(nn', q, \omega_0) - \Pi_2(nn', q, \omega_0 + \omega)\right] \\ \times \left[2n\left(\frac{\omega_0 + \omega}{T_e}\right) + 1\right], \end{aligned} \tag{3.22}$$

$$\begin{aligned} S^{ph}(\omega) = -\frac{1}{2NS}\sum_{\mathbf{q}q_z\lambda nn'} q_\alpha^2 |M_{nn'}(\mathbf{Q}, \lambda)|^2 \left\{\Pi_2(nn', q, \Omega_{Q\lambda} + \omega_0 + \omega)\left[\coth\left(\frac{\Omega_{Q\lambda} + \omega_0 + \omega}{2T_e}\right) \times \right.\right. \\ \left.\coth\left(\frac{\Omega_{Q\lambda}}{2T}\right) - 1\right] - \Pi_2(nn', q, \Omega_{Q\lambda} + \omega_0 - \omega)\left[\coth\left(\frac{\Omega_{Q\lambda} + \omega_0 - \omega}{2T_e}\right)\coth\left(\frac{\Omega_{Q\lambda}}{2T}\right) - 1\right]\Bigg\}, \end{aligned} \tag{3.23}$$

$$M_2^i(\omega) = \frac{1}{\omega mNS}\sum_{\mathbf{q}nn'} \frac{q_\alpha^2}{q^2} |U_{nn'}(q)|^2 \left[\Pi_2(nn', q, \omega_0) - \Pi_2(nn', q, \omega_0 + \omega)\right], \tag{3.24}$$

$$\begin{aligned} M_2^{ph}(\omega) = \frac{1}{\omega mNS}\sum_{\mathbf{q}q_z\lambda nn'} q_\alpha^2 |M_{nn'}(\mathbf{Q}, \lambda)|^2 \left\{\Pi_2(nn', q, \Omega_{Q\lambda} + \omega_0 + \omega)\left[n\left(\frac{\Omega_{Q\lambda} + \omega_0 + \omega}{T_e}\right)\right.\right. \\ \left.\left. -n\left(\frac{\Omega_{Q\lambda}}{T}\right)\right] - \Pi_2(nn', q, \Omega_{Q\lambda} + \omega_0 - \omega)\left[n\left(\frac{\Omega_{Q\lambda} + \omega_0 - \omega}{T_e}\right) - n\left(\frac{\Omega_{Q\lambda}}{T}\right)\right]\right\}, \end{aligned} \tag{3.25}$$

with $\omega_0 \equiv q_x v_d$ and the area of the junction S. In these equations, $\alpha = x$ (or y) corresponds to the longitudinal (or transverse) component. T and $\Omega_{Q\lambda}$ are lattice temperature and phonon energy of wave vector $\mathbf{Q}$ (three-dimensional wave vector $(\mathbf{q}, q_z)$), branch λ, respectively. $U_{nn'}(q)$ and $M_{nn'}(\mathbf{Q}, \lambda)$ denote the matrix elements of the electron-impurity and electron-phonon interactions respectively.[38]

Employing above formulation, we have taken the GaAs-AlGaAs heterojunction system with only the lowest and next lowest subbands occupied as an example to calculate the thermal-noise temperature as a function of dc bias points in the lattice temperature $T = 80\ K$. Thus the random phase approximation Eq.(3.19) can be truncated by taking $n, n', m, m' = 0, 1$ only. In the evaluation, we neglect the contribution of the electron-impurity scattering for the sake of simplicity and it would not lose the qualitative understanding about the thermal-noise problem. Moreover, both the electron-acoustic-phonon interaction (via piezoelectric coupling and deformation potential) and electron-polar-optical-phonon interaction (via Fröhlich coupling) are considered in the calculation and the electron-phonon matrix elements $M_{nn'}(\mathbf{Q}, \lambda)$ are given as:

$$M_{nn'}(\mathbf{Q}, \lambda) = M(\mathbf{Q}, \lambda) I_{nn'}(iq_z).$$

$M(\mathbf{Q}, \lambda)$ is the matrix element of the electron-phonon interaction in the three-dimensional plane-

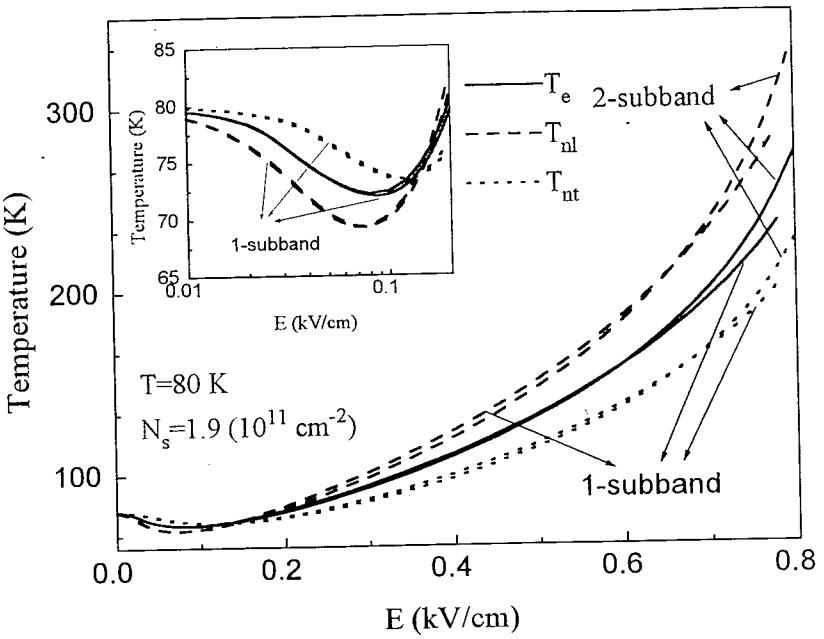

Figure 3-4: The electron temperature T_e (solid curves) and the longitudinal (dashed curves) and transverse (dotted curves) noise temperatures T_{nl} and T_{nt} at $\omega \sim 0$ are depicted as functions of bias dc fields for a GaAs-AlGaAs heterojunction with electron sheet density $N_s = 1.9 \times 10^{11}$ cm^{-2} at lattice temperature $T = 80$ K for the cases of one- and two-subband occupation. In the inset, the same quantities are replotted at low electric field range in order to display them in detail.

wave representation, and $I_{nn'}(iq_z)$ the form factors of the electron-phonon interaction of quasi-two-dimensional heterojunction systems which can be determined by:[37]

$$I_{nn'}(iq_z) = \int e^{-iq_z z} \zeta_n^*(z) \zeta_{n'}(z) dz.$$

In Figs.3-4 and 3-5 we present the longitudinal and transverse noise temperatures T_{nl} (dashed lines) and T_{nt} (dotted lines) at $\omega \sim 0$, as well as the electron temperature T_e (solid lines), as functions of the bias dc fields E for samples with different electron sheet densities $N_s = 1.9$ and 5.7×10^{11} cm^{-2}, respectively, whose typical energy gaps between the lowest and the next lowest subbands ($\varepsilon_1 - \varepsilon_0$) are 8 meV and 31 meV by means of the variational calculation, respectively. For comparison, those results corresponding to the same samples assumed only the lowest subband occupied are also plotted in the figures. First of all, we can see easily from the two figures that occupation of more than the lowest subband reproduces the features for the case of one-subband occupation that the cooling effect, all T_e, T_{nl} and T_{nt} can be lower than the lattice temperature T, shows up over wide ranges of dc bias, and at lower dc bias T_{nl} is lower than T_{nt}, whereas at higher dc bias T_{nl} is higher than T_{nt}, as well as T_{nl} or T_{nt} is respectively higher or lower than the electron temperature T_e at strong electric field range. However, the difference between the results of the one- and two-subband occupation is obvious, especially for the case of higher electron density. It is very clear in the Fig.3-5 that a large decrease of the electron temperature and noise temperatures by a nearly half of magnitude of those of the one-subband occupation at the strong electric field region attributes to including the next lowest subband in spite of a considerable great energy gap. On the contrary, only slight deviation is found for the low electron density $N_s = 1.9 \times 10^{11}$ cm^{-2} (Fig.3-4) even under high electric fields. This is because the system with high electron density possesses high Fermi energy level and electrons can easily be excited into the next lowest subband even though a weak external electric field is added. Thus we can draw conclusion from the numerical result that higher the electron density is,

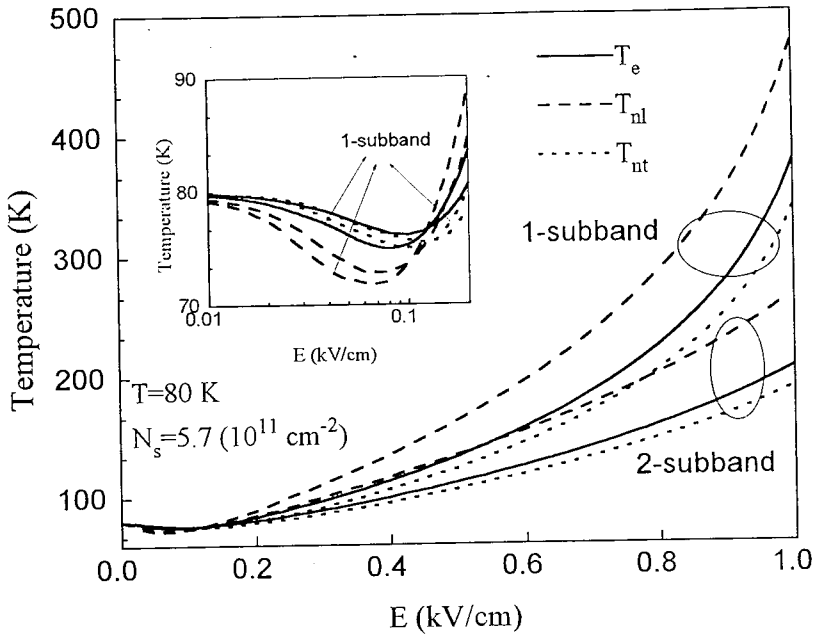

Figure 3-5: The same as Fig.3-4 except for electron density of 5.7×10^{11} cm^{-2}.

greater disparity is found and that it is necessary to consider occupation of multiple subbands for sufficiently high electron densities in order to properly investigate the transport properties of quasi-two-dimensional heterojunction systems. In addition, the insets in the two figures demonstrate clearly another interesting feature that including the next lowest subband inclines to reduce the cooling effect.

Chapter 4

Hole Perpendicular Transport of Superlattice Systems

4.1 Background

Since Esaki and Tsu[56] proposed the concept of superlattice structure more than twenty years ago, there has been an intensified interest in theoretical and experimental studies of the carrier transport in a direction perpendicular to the quantum-well layers because of the prospect of a negative differential conductance (NDC). In recent years, the NDC has been experimentally observed by Sibille *et al.* [57] and Grahn *et al.*[58] in dc perpendicular transport in GaAs superlattices (SL's) having wide range of miniband widths, and attributed to Bloch electron conduction through the superlattice miniband as predicted by Esaki and Tsu[56]. At the same time, superlattice miniband transport has been further studied theoretically using balance-equation[59] and Boltzmann equation[60, 61] approaches.

However, most of these studies were aimed at the electron transport, although several experiments have vindicated the truth that holes play a great role in the carrier transport properties of superlattices. For example, by measuring subpicosecond luminescence spectra, Deveaud *et al.* [62] have found that the perpendicular transport of electrons and holes is Bloch transport for 20/20 and 10/10 SL's, and observed a dramatic decrease in mobility in the 30/30 SL compared to that in the 20/20 SL resulting from an order-of-magnitude reduction in the hole miniband width. Furthermore, Fujiwara and his collaborators[7] have studied the correlation between the temperature-dependent transport processes in superlattices and the miniband width by varying only the barrier thickness. Their experimental results have clearly shown that *the ambipolar transport is operative at carrier densities in excess of* $10^{15} - 10^{17}$ cm^{-3}. Unfortunately, the profound energy spectrum caused by the complex nature of hole wave functions hinders the theoretical investigation of the transport of holes in the SL's and numerical calculations for the perpendicular transport of holes in other structures (such as double-barrier and double-quantum-well structures) have proved the fact that the effects of heavy-hole–light-hole mixing are very important. In order to overcome the difficulties, an analytical approach basing on the strong difference between the heavy-hole (hh) and light-hole (lh) effective masses has recently been developed by Raichev[64] and an approximation expression for the energy spectrum of the holes in the lowest miniband which can describe the effects of hh-lh mixing has been obtained. Using this hole spectrum, he evaluated the linear conductivity and diffusion coefficients of the hole in SL's with different superlattice periods within the Kubo formalism, assuming that holes are scattered only by the static disorder impurity potential. The purpose of the paper is to examine this problem by means of the extended balance equation approach[59], which enables us to analyze the transport behavior of holes in SL's under strong dc electric fields and to take into account realistic scattering mechanisms (i.e., the hole-impurity and hole-phonon interaction).

First, a brief discussion about the extended Lei-Ting balance equation approach for an arbitrary energy band and its application to investigation of miniband transport of electron in superlattices has been performed. In the following, we have derived an analytical expression for the energy spectrum of holes in the lowest miniband. Finally, numerical calculations about the miniband transport of holes in superlattices have been carried out and remarked.

4.2 Balance Equation Theory for an Arbitrary Energy Band

For nonparabolic bands, the motion of center-of-mass can not be separated completely from the relative motion of the electrons due to the nonparabolicity of energy bands. However, considering the great difference of masses between the center-of-mass and relative electrons, we can separated them approximately following the spirit of the adiabatic approximation as we deal with electrons and ions in solids. The center-of-mass momentum is used to describe the motion of the center-of-mass in the presence of the external fields. With this in mind, the density matrix is chosen as[24, 59]

$$\hat{\rho}_0 = e^{-H_e/T_e}|\mathbf{P}_d\rangle\langle\mathbf{P}_d|. \tag{4.1}$$

Here $|\mathbf{P}_d\rangle$ is a single particle (center-of-mass) state bearing an average c.m. momentum $\mathbf{P}_d$ in the presence of the electric field.

$$H_e = \sum_{\mathbf{k},\sigma} \varepsilon(\mathbf{k}-\mathbf{p}_d) c^\dagger_{\mathbf{k}\sigma} c_{\mathbf{k}\sigma} + H_{ee} \tag{4.2}$$

is the relative electron Hamiltonian. The center-of-mass momentum $\mathbf{P}_d = N\mathbf{p}_d$, and the electron temperature T_e are used as fundamental parameters.

In nonparabolic band case, the effective mass is function of the electron energy. An ensemble-averaged effective-mass tensor, $\mathcal{K}$, is introduced to carry the major part of the nonparabolic effect on transport, which is defined by

$$\mathcal{K} = \frac{2}{N}\sum_{\mathbf{k}} \nabla\nabla\varepsilon(\mathbf{k}) f(\bar{\varepsilon}(\mathbf{k}), T_e). \tag{4.3}$$

Nonparabolicity also showes up through the energy function $\varepsilon(\mathbf{k})$ and the velocity function $\mathbf{v}(\mathbf{k}) \equiv \nabla\varepsilon(\mathbf{k})$. The average drift velocity of the electron system is given by

$$\mathbf{v}_d = \frac{2}{N}\sum_{\mathbf{k}} \nabla\varepsilon(\mathbf{k}) f(\bar{\varepsilon}(\mathbf{k}), T_e). \tag{4.4}$$

The force and energy balance equations for a nonparabolic band take the form

$$e\mathbf{E}\cdot\mathcal{K} + \mathbf{A}_i + \mathbf{A}_p = 0. \tag{4.5}$$

$$e\mathbf{E}\cdot\mathbf{v}_d - W = 0. \tag{4.6}$$

The accelerations due to impurity and phonon scatterings, $\mathbf{A}_i$ and $\mathbf{A}_p$, and the energy dissipation rate W, are respectively:

$$\mathbf{A}_i = \frac{2\pi n_i}{N}\sum_{\mathbf{k},\mathbf{q}} |u(\mathbf{q})|^2 |g(\mathbf{k},\mathbf{q})|^2 [\mathbf{v}(\mathbf{k}+\mathbf{q}) - \mathbf{v}(\mathbf{k})] \delta(\varepsilon(\mathbf{k}+\mathbf{q}) - \varepsilon(\mathbf{k})) \times \frac{f(\bar{\varepsilon}(\mathbf{k}), T_e) - f(\bar{\varepsilon}(\mathbf{k}+\mathbf{q}), T_e)}{|\epsilon(\mathbf{q}, \varepsilon(\mathbf{k}) - \varepsilon(\mathbf{k}+\mathbf{q}))|^2}, \tag{4.7}$$

$$\mathbf{A}_p = \frac{4\pi}{N}\sum_{\mathbf{k},\mathbf{q},\lambda} |M(\mathbf{q},\lambda)|^2 |g(\mathbf{k},\mathbf{q})|^2 [\mathbf{v}(\mathbf{k}+\mathbf{q}) - \mathbf{v}(\mathbf{k})]\, \delta(\varepsilon(\mathbf{k}+\mathbf{q}) - \varepsilon(\mathbf{k}) + \Omega_{\mathbf{q}\lambda}) \times \frac{f(\bar{\varepsilon}(\mathbf{k}),T_e) - f(\bar{\varepsilon}(\mathbf{k}+\mathbf{q}),T_e)}{|\epsilon(\mathbf{q},\bar{\varepsilon}(\mathbf{k}) - \bar{\varepsilon}(\mathbf{k}+\mathbf{q}))|^2} \left[n\left(\frac{\Omega_{\mathbf{q}\lambda}}{T}\right) - n\left(\frac{\bar{\varepsilon}(\mathbf{k}) - \bar{\varepsilon}(\mathbf{k}+\mathbf{q})}{T_e}\right)\right], \tag{4.8}$$

$$W = \frac{4\pi}{N}\sum_{\mathbf{k},\mathbf{q},\lambda} |M(\mathbf{q},\lambda)|^2 |g(\mathbf{k},\mathbf{q})|^2 \Omega_{\mathbf{q}\lambda}\, \delta(\varepsilon(\mathbf{k}+\mathbf{q}) - \varepsilon(\mathbf{k}) + \Omega_{\mathbf{q}\lambda}) \times \frac{f(\bar{\varepsilon}(\mathbf{k}),T_e) - f(\bar{\varepsilon}(\mathbf{k}+\mathbf{q}),T_e)}{|\epsilon(\mathbf{q},\bar{\varepsilon}(\mathbf{k}) - \bar{\varepsilon}(\mathbf{k}+\mathbf{q}))|^2} \left[n\left(\frac{\Omega_{\mathbf{q}\lambda}}{T}\right) - n\left(\frac{\bar{\varepsilon}(\mathbf{k}) - \bar{\varepsilon}(\mathbf{k}+\mathbf{q})}{T_e}\right)\right], \tag{4.9}$$

with $\bar{\varepsilon}(\mathbf{k}) = \varepsilon(\mathbf{k} - \mathbf{p}_d)$ being the relative electron energy. Now the steady-state balance equations (4.5) and (4.6), together the condition that the total number of the electrons equals N:

$$N = 2\sum_{\mathbf{k}} f(\bar{\varepsilon}(\mathbf{k}), T_e), \tag{4.10}$$

can determine the dc drift velocity and the electron temperature under the influence of a constant electric field.

Applying the balance equations for an arbitrary energy band system, we can investigate the Bloch electron conductivity in a superlattice miniband, the extremly nonparabolic case. Assuming that the conducting carriers of the superlattice are free to move in layers (x-y plane), but are subject to a periodic potential in the z direction, with the single-electron state described by a wave vector $\mathbf{k} = (\mathbf{k}_\parallel, k_z)$, $-\pi/d < k_z \leq \pi/d$, d being the period of the superlattice. A tight-binding model is employed for the energy dispersion relation $\varepsilon(\mathbf{k}) = k_\parallel^2/2m + \varepsilon_1(k_z)$ with

$$\varepsilon_1 = \frac{1}{2}\Delta\,(1 - \cos(k_z d))\,. \tag{4.11}$$

Δ being the miniband width. Under the influence of a uniform electric field along the z direction, the ensemble-averaged inverse-effective-mass tensor $\mathcal{K}$ becomes $\mathcal{K}_{xx} = \mathcal{K}_{yy} = 1/m$, $\mathcal{K}_{i\neq j} = 0$, and

$$\mathcal{K}_{zz} = \frac{2}{N}\sum_{\mathbf{k}} \frac{d^2\varepsilon_1(k_z)}{dk_z^2} f(\bar{\varepsilon}(\mathbf{k}), T_e) = \frac{\Delta d^2}{N}\sum_{\mathbf{k}} \cos(k_z d) f(\bar{\varepsilon}(\mathbf{k}), T_e), \tag{4.12}$$

where $\bar{\varepsilon}(\mathbf{k}) = \varepsilon_{\mathbf{k}_\parallel} + \varepsilon_1(k_z - p_d)$ is the energy of the relative electrons. Moreover, the average drift velocity of the carrier system in the z direction equals

$$v_d = \frac{\Delta d}{N}\sum_{\mathbf{k}} \sin(k_z d) f(\bar{\varepsilon}(\mathbf{k}), T_e). \tag{4.13}$$

The balance equations (4.5) and (4.6) have been solved numerically for p_d and T_e as functions of the electric field E at various lattice temperatures T, carrier sheet densities N_s, superlattice periods d, and miniband widths Δ with parameters pertinent to the Γ-valley electrons in the GaAs/AlAs superlattice. Scatterings due to impurities, polar-optic phonons, and acoustic phonons (including deformation potential and piezoelectric couplings) are taken into account. At first, the dependence of drift velocity v_d and electron temperature T_e on the external electric field has been investigated for several different miniband widths and all the velocity-field curves exhibit negtive differential conductance with peak velocities v_p at critical fields E_c as expected by Esaki and Tsu. However, different from the single electron model of Esaki and Tsu which predicts that the same dependence of (v_d/v_p) as a function of (E/E_c) is independent of the superlattice period d, miniband width Δ, and temperature T, the balance equation method has found that miniband width Δ playes a great role in determining the peak velocity v_p. To compare with the experiments of Sibille *et al.*, the peak velocities v_p/d and critical fields $E_c d$ are calculated for different miniband widths Δ and the theoretical results are in

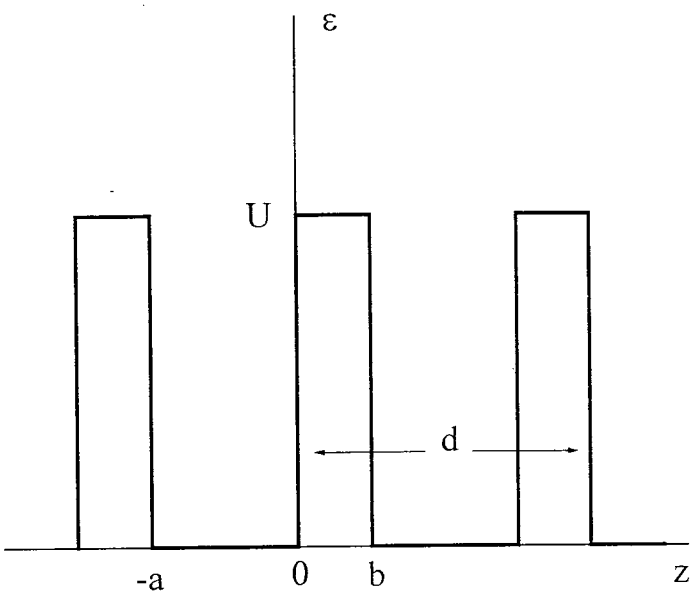

Figure 4-1: Potential diagram of the superlattice. a and b are the well and barrier widths, respectively. d is the superlattice period.

remarkably good agreement with the experimental data. Moreover, the temperature dependence of linear mobility and velocity-field behavior has been studied. The balance equation theory predicts widely varying temperature- and miniband-width-dependent nonlinear velocity-field behavior.

4.3 Hole Bloch Transport in Superlattices

In order to study hole transport in a superlattice (SL), we must first investigate the spectrum of the hole energy band. Assume that the conducting carriers of the GaAs-AlGaAs SL's are free to move in layers (x–y plane), but are subject to a periodic potential $U(z)$ (Krönig-Penney potential) in the z direction as depicted in Fig.4-1 (a and b stand for the well and barrier widths, respectively. d is the superlattice period.). According to the treatment of Raichev[64], the isotropic Luttinger Hamiltonian[65] is used to describe hole states in this system. The isotropic Luttinger Hamiltonian is used to describe hole states in superlattices:

$$\left[-\frac{1}{2m_h}\frac{\partial^2}{\partial z^2}-\frac{3}{8m_l}\left[1+\frac{m_l}{3m_h}\right]\frac{\partial^2}{\partial \mathbf{r}_\parallel^2}+U(z)-\varepsilon\right]\begin{bmatrix}\Psi_\lambda^1(\mathbf{r}_\parallel,z)\\ \\ \Psi_\lambda^4(\mathbf{r}_\parallel,z)\end{bmatrix}$$

$$=\frac{\sqrt{3}}{8m_l}\left(1-\frac{m_l}{m_h}\right)\begin{bmatrix}2k_-\dfrac{\partial}{\partial z} & -k_-^2\\ \\ -k_+^2 & 2k_+\dfrac{\partial}{\partial z}\end{bmatrix}\begin{bmatrix}\Psi_\lambda^2(\mathbf{r}_\parallel,z)\\ \\ \Psi_\lambda^3(\mathbf{r}_\parallel,z)\end{bmatrix}. \tag{4.14}$$

$$\left[-\frac{1}{2m_l}\frac{\partial^2}{\partial z^2}-\frac{3}{8m_l}\left[\frac{1}{3}+\frac{m_l}{m_h}\right]\frac{\partial^2}{\partial \mathbf{r}_{\|}^2}+U(z)-\varepsilon\right]\begin{bmatrix}\Psi_\lambda^2(\mathbf{r}_{\|},z)\\ \Psi_\lambda^3(\mathbf{r}_{\|},z)\end{bmatrix}$$

$$=\frac{\sqrt{3}}{8m_l}\left(1-\frac{m_l}{m_h}\right)\begin{bmatrix}-2\hat{k}_+\frac{\partial}{\partial z} & -\hat{k}_-^2\\ -\hat{k}_+^2 & -2\hat{k}_-\frac{\partial}{\partial z}\end{bmatrix}\begin{bmatrix}\Psi_\lambda^1(\mathbf{r}_{\|},z)\\ \Psi_\lambda^4(\mathbf{r}_{\|},z)\end{bmatrix} \tag{4.15}$$

where $\mathbf{x}=(x,y)$, $\hat{k}_\pm=-i(\partial/\partial y)\pm(\partial/\partial y)$, m_h and m_l are the heavy-hole (hh) and light-hole (lh) effective masses, respectively. Transmission the (**x**,z) representation to the mixed ($\mathbf{k}_{\|},z$) ($\mathbf{k}_{\|}$ is the two-dimensional plane wave vector and $\mathbf{k}=(\mathbf{k}_{\|},k_z)$) representation, considering the strongly different effective masses between the hh m_h and the lh m_l ($m_l/m_h\ll 1$) and restricting $k_{\|}$ to satisfy the following requirements:

$$k_{\|}^2\ll\frac{m_l}{m_h}\frac{\pi^2}{d^2}, \tag{4.16}$$

we can write the hole wave function as following:

$$\Psi_\lambda(\mathbf{k}_{\|},z)=\frac{1}{\sqrt{N_0}}\sum_{k_z,N}F_{k_{\|},k_z}(z-dN)e^{ik_zdN}\varphi^\lambda_{\mathbf{k}_{\|},k_z}, \tag{4.17}$$

where N number the SL periods and N_0 is the total number of periods. $F_{k_{\|},k_z}(z)$ is defined in the interval $z\in[-a,b]$. Finally, we obtain that the function $\varphi^\lambda_{\mathbf{k}_{\|},k_z}$ satisfies

$$\left[\varepsilon(\mathbf{k}_{\|},k_z)-\varepsilon\right]\varphi^\lambda_{\mathbf{k}_{\|},k_z}=0. \tag{4.18}$$

Here $\varepsilon(\mathbf{k}_{\|},k_z)$ is the unperturbed energy spectrum of holes in the lowest miniband of the SL's. Considering the case of samll under-barrier penetration of the hole wave functions, i.e., $(\gamma b)^2\gg 1$ $\left[\gamma=(2m_hU)^{1/2}\right]$, an approximate expression for the hole spectrum of the lowest miniband is obtained in the following form: [66]

$$\varepsilon(\mathbf{k}_{\|},k_z)=\frac{\Delta}{2}\left[1-\cos(k_zd)\right]+\frac{3k_{\|}^2}{m_l\pi^2R(k_z)}, \tag{4.19}$$

where $\Delta\simeq\left(8\pi^2/m_h\gamma a^3\right)\exp(-\gamma b)$ is the miniband width at $k_{\|}=0$. Function $R(k_z)$ is defined as

$$R(k_z)=R_0\left[1-\alpha\cos(k_zd)\right], \tag{4.20}$$

in which $R_0=1+2\coth(\kappa b)/\kappa a$ and $\alpha=2/R_0\kappa a\sinh(\kappa b)$ $\left[\kappa^2=2m_lU\right]$. It is obvious that the derived hole spectrum is different from the conventional tight-binding energy spectrum and that the $k_{\|}$-dependent part of the energy spectrum also depends on the transverse wave number k_z, which describes the effect of admixture of hh-lh on the energy spectrum. In the limit of $\alpha=0$, this energy spectrum Eq.(4.19) reduces to the conventional electron-like dispersion relation, i. e. neglects the effect of the hh-lh mixing.

The force and energy balance equations for steady-state transport when a uniform electric field **E** is applied along the z direction are[24]

$$eE/m_z^*+A_i+A_p=0, \tag{4.21}$$

$$eEv_d - W = 0. \tag{4.22}$$

Here A_i and A_p represent the frictional accelerations due to impurity and phonon scatterings and W is the hole energy-loss rate (per carrier) due to hole-phonon interaction. Two parameters, the center-of-mass momentum $P_d \equiv Np_d$ and the hole temperature T_h are used to describe the transport state of the system. The statistically averaged inverse effective mass is

$$\frac{1}{m_z^*} = \frac{2}{N}\sum_{\mathbf{k}} \frac{d^2\varepsilon(\mathbf{k}_\parallel, k_z)}{dk_z^2} f\left(\varepsilon(\mathbf{k}_\parallel, k_z - p_d), T_h\right), \tag{4.23}$$

and the drift velocity is given by

$$v_d = \frac{2}{N}\sum_{\mathbf{k}} v(\mathbf{k}) f\left(\varepsilon(\mathbf{k}_\parallel, k_z - p_d), T_h\right), \tag{4.24}$$

where $v(\mathbf{k}) = d\varepsilon(\mathbf{k}_\parallel, k_z)/dk_z$ is the velocity function in the z direction, and all the other physical quantities are functions of p_d and T_h. In the above equations

$$f\left(\varepsilon(\mathbf{k}_\parallel, k_z), T_h\right) = \left[\exp\left((\varepsilon(\mathbf{k}_\parallel, k_z) - \mu)/T_h\right) + 1\right]^{-1} \tag{4.25}$$

is the Fermi distribution function at the hole temperature T_h, μ is the chemical potential determined by the total number of particle $N = 2\sum_{\mathbf{k}} f\left(\varepsilon(\mathbf{k}_\parallel, k_z), T_h\right)$. The expressions for A_i, A_p and W are the same as those given in the above section except for T_e being replaced by T_h.

4.4 Discussion

Numerical investigation of the perpendicular transport properties of holes are presented in the following for GaAs-AlGaAs SL's with and without the effect of hh-lh mixing, which are obtained by solving Eqs.(4.21) and (4.22). In the calculation, hole-impurity, hole-polar-optic-phonon, and hole-nonpolar-optic-phonon interactions are taken into account and hole-acoustic-phonon (deformation potential and piezoelectric) scatterings are neglected because of their tiny contributions at the considered temperature. For simplicity, phonon modes are assumed to be three dimensional. The material constants are typical values of GaAs. The valence-band offset in the GaAs-$Al_{0.3}Ga_{0.7}As$ heterostructure is chosen as $U = 0.16$ eV. In our theory, the only adjustable parameter involved is the impurity scattering rate or the impurity density. At low temperature, the mobility of SL's is impurity-limited, so that we can define this parameter. Deveaud *et al.* have deduced in Ref.[62] that the hole weak-field mobility in the measured 20/20 SL is 900 $cm^2/V{\cdot}s$ at the lattice temperature of 15 K. Here we adjust the impurity density to fit the experimental data for the same family of SL's with hole density 1×10^{17} cm^{-3} at 15 K. Using the same material constants and impurity density, we calculate the hole mobility for the 30/30 SL with the common hole density to be 42 $cm^2/V{\cdot}s$, which is very close to Deveaud's measured 50 $cm^2/V{\cdot}s$[62]. On the contrary, if we neglect the effect of hh-lh mixing by setting $\alpha = 0$ in the Eq.(4.20), a calculated hole mobility which is nearly two times as high as the experimental data for the 30/30 SL is obtained through the same procedure. This comparison show that neglecting the effect of hh-lh mixing is inconsistent with available experimental data.

First we study the linear transport. Figs.4-2 describes the dependence of impurity-limited hole mobility on the hole density at 15 K for the 20/20 ($d = 4$ nm) and the 30/30 ($d = 6$ nm) SL's, assuming the hole mobility at 1×10^{17} cm^{-3} to be 900 $cm^2/V{\cdot}s$ for the 20/20 SL and 42 $cm^2/V{\cdot}s$ for the 30/30 SL respectively. In this and following figures, the solid lines represent the calculations which take into account the effect of hh-lh mixing on the hole transport, while the dashed lines correspond to the case of neglecting this effect ($\alpha = 0$). There is only trivial difference between the calculations at $\alpha = 0.618$ and the calculations at $\alpha = 0$ for the 20/20 SL within the whole range of densities, but this disparity

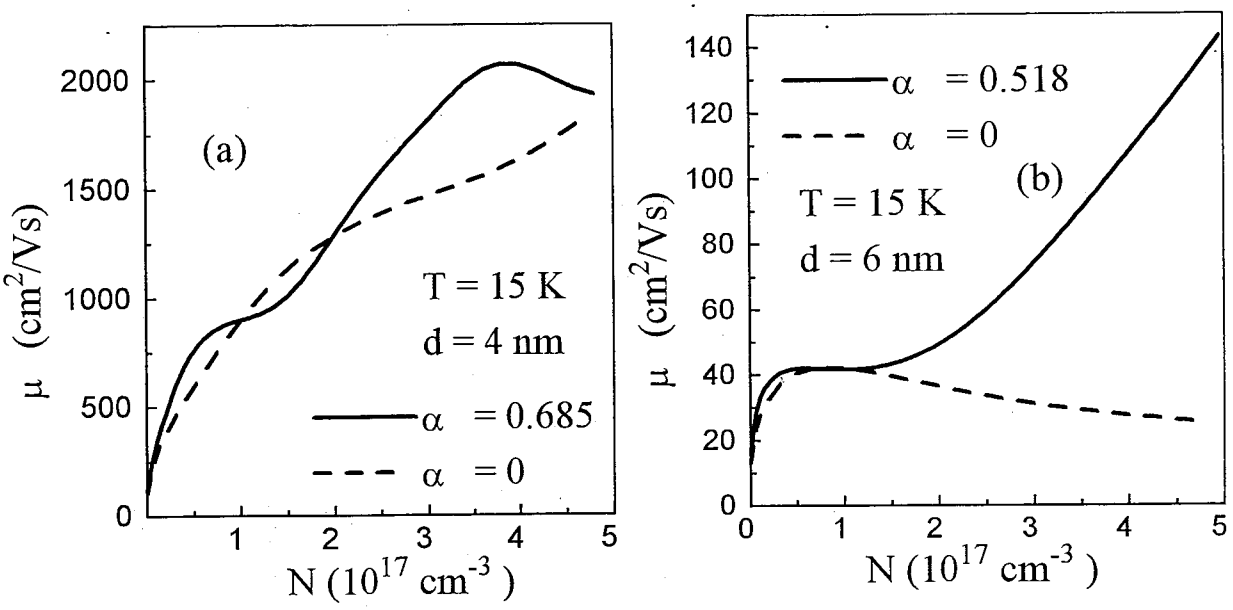

Figure 4-2: The dependence of the weak-field hole mobility on the hole density is shown for the (a) 20/20 (d = 4 nm) and (b) 30/30 (d = 6 nm) GaAs-AlGaAs SL's at the lattice temperature of 15 K, including (α = 0.685 for 20/20 SL and α = 0.518 for 30/30 SL) and excluding (α = 0 for both SL's) the effect of hh-lh mixing. Assume the weak-field hole mobilities of the 20/20 and 30/30 SL's at density 1×10^{17} cm^{-3} is 900 cm^2/V·s and 42 cm^2/V·s, respectively.

becomes evident for the 30/30 SL, such is consistent with Raichev's results of the conductivity and the diffusion coefficient versus the hole density at zero temperature.[64] In the 20/20 SL, the hole mobility increases monotonously with increasing density due to its wide miniband if the effect of hh-lh mixing is not considered. However, if taking into account hh-lh mixing the calculated result exhibits a peak of mobilities at about 4×10^{17} cm^{-3}. On the contrary, the electron-like mobilities for the 30/30 SL with a narrow miniband arrive at a peak at about 1×10^{17} cm^{-3} and decrease slowly with the increase of the densities. The calculated mobilities with considering hh-lh mixing increase rapidly when the density is higher than 1.5×10^{17} cm^{-3}.

In Figs.4-3, perpendicular velocities and hole temperatures in the 20/20 and the 30/30 SL's with hole concentration 1×10^{17} cm^{-3} are illustrated as functions of electric fields at the lattice temperature of 140 K. In order to satisfy the requirement Eq.(4.16), we restrict the electric fields less than 20 and 15 kV/cm, respectively, to ensure that more than 80% of the total holes dwell in the states of $k^2 < 0.2\,(m_l/m_h)\,(\pi^2/d^2)$. A significant result is that the negative differential conductance (NDC) disappears for the hot-hole perpendicular transport in both types of SL's due to the effect of hh-lh mixing in comparison with the electron-like calculated results ($\alpha = 0$), where NDC shows up for both systems. Another feature is that the hole temperature is generally much lower in the case considering hh-lh mixing than in the case without mixing at small to medium strengths of the electric field. In the 20/20 SL system, an appreciable cooling ($T_h < T$) shows up around $E \sim 6$ kV/cm.

Summing up, the effect of hh-lh mixing plays a significant role in both linear and nonlinear hole transport in SL's. And the negative differential conductance of perpendicular transport of holes is broken down due to this effect.

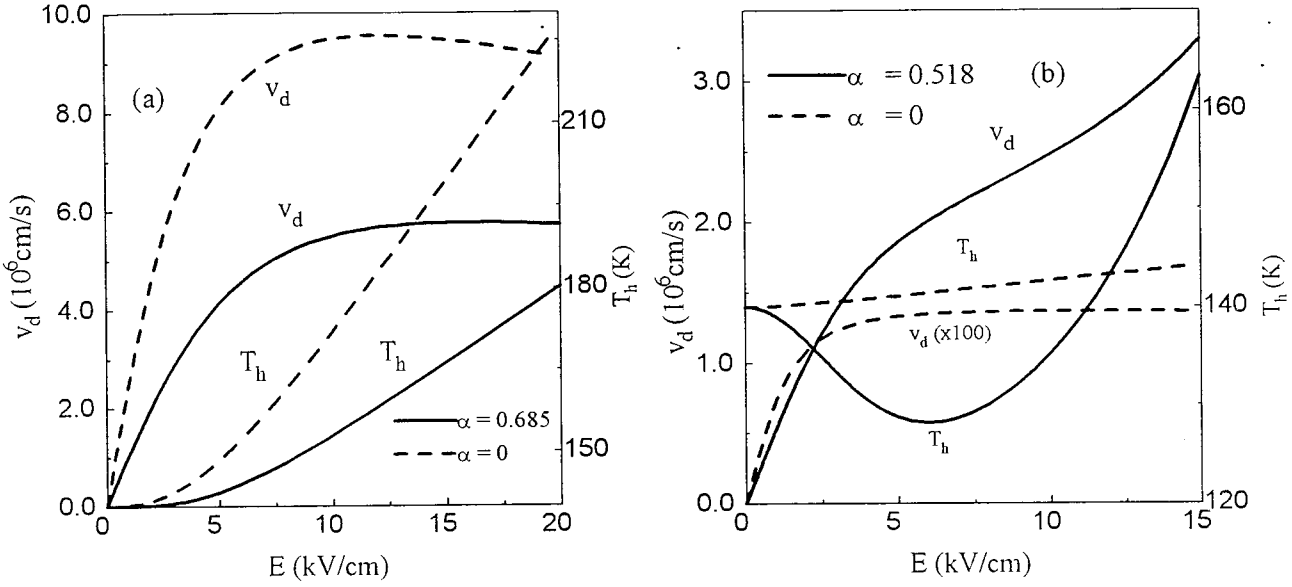

Figure 4-3: The calculated drift velocities and hole temperatures of hot-hole in the (a) 20/20 (d = 4 nm) and (b) 30/30 (d = 6 nm) GaAs-AlGaAs SL with hole density 1×10^{17} cm^{-3} are shown as functions of the electric fields at lattice temperature of 140 K. Both the results with ($\alpha = 0.685$ in (a) and $\alpha = 0.518$ in (b)) and those without ($\alpha = 0$) the effect of hh-lh mixing are plotted.

Chapter 5

Summary

Multivalley or multisubband occupations of carriers are believed to play an important role in determining high field transport propertites of bulk and low-dimensional semiconductor systems. In low-dimensional systems, the scattering rates assoiated with intersubband transition, such as intersubband electron-impurity, electron-phonon and electron-electron interactions, have been enormously discussed. In these literature, carriers populated in different subbands have been assumed to share a common energy due to the unique electron effective mass in different subbands and treated as a single type of carriers. Some authors have argued that the inelastic scattering, i.e., intersubband electron-electron Coulomb interaction, allows energy to be transferred from hot subbands to cold subbands so that a uniform energy is quickly reached between different subbands under an external electric field. This presumption is worth deliberately consulting because the intra- and inter-subbnad electron-electron Coulomb interactions depend strongly on the dimensionality of the system and density of carriers.

Unfortunately, a detailed proof of this presumption is lacking. Therefore in the thesis, a systematically investigation of the effect of intersubband scatterings, especially the intersubband electron-electron Coulomb interaction, on the linear and nonlinear transport properties for systems of different dimensionality and having different carrier densities of quasi-two-dimensional and quasi-one-dimensional electron systems has been performed by employing the Lei-Ting balance-equations approach of two-types-of-carriers model (TTCM) to treat the GaAs-based model systems having two subbands. According to TTCM of Lei-Ting balance-equations approach, which is developed to deal with the high field transport properties of semiconductors with multi-valley occupancy, electrons within the same subband are treated as a single type of carriers due to enough strong intrasubband electron-electron Coulomb interactions, but electrons in different subbands are taken as two types of carriers and posses different drift velocities, electron temperatures and chemical potentials. Thus we can focus our attention on the role of the dominate intersubband electron-electron Coulomb interaction in transport. Numerous investigations show that electrons between the different subbands can not generally achieve a common energy under an external electric field in spite of inter-subband energy exchange. When the electron density rises, the inter-subband Coulomb interaction, i.e., inter-subband energy exchange, is enhanced and does make the electrons dwelling in different subbands thermalize and reach a common drift velocity and electron temperature. Hence electrons in different subbands can be considered as a single type of carriers and OTCM is a good approximation for this low-dimensional systems with high electron densities. Moreover, confinement of low-dimensional systems can alter the threshold of electron density for the validity of OTCM. By analyzing the linear mobility in quantum wells, we demonstrate that the real mobility tends to the result μ_B of the two-band model of Boltzmann equation in the limit of weak intersubband electron-electron Coulomb interaction, and on the contrary, it tends to the Lei-Ting mobility μ_L of OTCM in the regime of strong intersubband electron-electron scattering. In addition, we argue that temperatures can alter the relative strength between

the electron-impurity and the inter-subband electron-electron interactions and hence determine the validity of OTCM. It is a direct deduction that for a clean sample the μ_B and the μ_L are equal even at extremely low temperature. Finally, we point out that the dominate intersubband Coulomb interaction can not make electrons in different subbands achieve a common chemical potential because of the interaction term not involving exchange of particles between different subbands.

Thermal-noise of hot electrons in semiconductors are known to be sensitive to details of band structure and scattering mechanisms. The same is true for electrons in a quasi-two-dimensional system. In the thesis, we have extended the theory of hot-electron thermal noise in quasi-two-dimensional systems based on the OTCM of the balance-equations to the case of multi-subband occupations and calculated the thermal-noise temperature of GaAs-GaAlAs heterjunction systems at different dc electric fields including the contributions of the lowest and next lowest subbands. We have found that, in comparison with the results of the one subband theory, the inclusion of a higher subband yields an electron density-dependent decrease of the electron temperature and the thermal-noise temperature and a reduction of the cooling effect.

Both linear and nonlinear hole perpendicular miniband transport in GaAs-based superlattices have been investigated by employing the balance eqution theory for miniband transport. Because of the profound energy spectrum resulting from the mixture of heavy-hole and light-hole, same novel transport properties have been discovered in comparison with electrons.

Appendix

The following table lists the material parameters of GaAs used in this thesis.

Parameter	value
optical dielectric constant κ_∞	10.8
low-frequency dielectric constant κ_0	12.9
effective mass of electron m^*	$0.067m_e$
effective mass of light hole m_l	$0.08m_e$
effective mass of heavy hole m_h	$0.5m_e$
mass density d	5.31 g/cm^3
longitudinal sound velocity v_{sl}	5.29×10^5 cm/s
transverse sound velocity v_{st}	2.48×10^5 cm/s
longitudinal optic phonon energy ω_{LO}	35.4 meV
acoustic deformation potential Ξ	8.5 eV
optic deformation potential D	3.0×10^8 eV/cm
piezoelectric constant e_{14}	1.41×10^9 V/m